Atmos. Chem. Phys., 13, 933–959, 2013
www.atmos-chem-phys.net/13/933/2013/
doi:10.5194/acp-13-933-2013

Atmospheric Chemistry and Physics

Aerosol particle measurements at three stationary sites in the megacity of Paris during summer 2009: meteorology and air mass origin dominate aerosol particle composition and size distribution

F. Freutel[1], J. Schneider[1], F. Drewnick[1], S.-L. von der Weiden-Reinmüller[1], M. Crippa[2], A. S. H. Prévôt[2], U. Baltensperger[2], L. Poulain[3], A. Wiedensohler[3], J. Sciare[4], R. Sarda-Estève[4], J. F. Burkhart[5], S. Eckhardt[5], A. Stohl[5], V. Gros[4], A. Colomb[6,7], V. Michoud[6], J. F. Doussin[6], A. Borbon[6], M. Haeffelin[8,9], Y. Morille[9,10], M. Beekmann[6], and S. Borrmann[1,11]

[1]Max Planck Institute for Chemistry, Mainz, Germany
[2]Laboratory of Atmospheric Chemistry, Paul Scherrer Institute, Villigen, Switzerland
[3]Leibniz Institute for Tropospheric Research, Leipzig, Germany
[4]Laboratoire des Sciences du Climat et de l'Environnement, Gif-sur-Yvette, France
[5]Norwegian Institute for Air Research, Kjeller, Norway
[6]LISA, UMR-CNRS 7583, Université Paris Est Créteil (UPEC), Université Paris Diderot (UPD), Créteil, France
[7]LaMP, Clermont Université, Université Blaise Pascal, CNRS, Aubière, France
[8]Institut Pierre-Simon Laplace, Paris, France
[9]Site Instrumental de Recherche par Télédétection Atmosphérique, Palaiseau, France
[10]Laboratoire de Météorologie Dynamique, Palaiseau, France
[11]Institute of Atmospheric Physics, Johannes Gutenberg University Mainz, Mainz, Germany

Correspondence to: J. Schneider (johannes.schneider@mpic.de)

Received: 25 July 2012 – Published in Atmos. Chem. Phys. Discuss.: 29 August 2012
Revised: 8 December 2012 – Accepted: 4 January 2013 – Published: 23 January 2013

Abstract. During July 2009, a one-month measurement campaign was performed in the megacity of Paris. Amongst other measurement platforms, three stationary sites distributed over an area of 40 km in diameter in the greater Paris region enabled a detailed characterization of the aerosol particle and gas phase. Simulation results from the FLEXPART dispersion model were used to distinguish between different types of air masses sampled. It was found that the origin of air masses had a large influence on measured mass concentrations of the secondary species particulate sulphate, nitrate, ammonium, and oxygenated organic aerosol measured with the Aerodyne aerosol mass spectrometer in the submicron particle size range: particularly high concentrations of these species (about 4 µg m^{-3}, 2 µg m^{-3}, 2 µg m^{-3}, and 7 µg m^{-3}, respectively) were measured when aged material was advected from continental Europe, while for air masses originating from the Atlantic, much lower mass concentrations of these species were observed (about 1 µg m^{-3}, 0.2 µg m^{-3}, 0.4 µg m^{-3}, and 1–3 µg m^{-3}, respectively). For the primary emission tracers hydrocarbon-like organic aerosol, black carbon, and NO_x it was found that apart from diurnal source strength variations and proximity to emission sources, local meteorology had the largest influence on measured concentrations, with higher wind speeds leading to larger dilution and therefore smaller measured concentrations. Also the shape of particle size distributions was affected by wind speed and air mass origin. Quasi-Lagrangian measurements performed under connected flow conditions between the three stationary sites were used to estimate the influence of the Paris emission plume onto its surroundings, which was found to be rather small. Rough estimates for the impact of the Paris emission plume on the suburban areas can be inferred from these measurements: Volume mixing ratios of 1–14 ppb of NO_x, and upper limits for mass concentrations of about 1.5 µg m^{-3} of black carbon and of about 3 µg m^{-3} of hydrocarbon-like organic aerosol can be

deduced which originate from both, local emissions and the overall Paris emission plume. The secondary aerosol particle phase species were found to be not significantly influenced by the Paris megacity, indicating their regional origin. The submicron aerosol mass concentrations of particulate sulphate, nitrate, and ammonium measured during time periods when air masses were advected from eastern central Europe were found to be similar to what has been found from other measurement campaigns in Paris and south-central France for this type of air mass origin, indicating that the results presented here are also more generally valid.

1 Introduction

As of 2011, for the first time the world's population exceeded the mark of 7 billion people. At the same time, more than 50 % of these people are living in a city, and this fraction is projected to be continuously increasing over the next decades (UN DESA, 2008, 2009). With this growing urbanization, also the cities themselves are becoming larger. While in 1950, only two cities worldwide had a population of more than 10 million inhabitants, today there are about twenty such cities worldwide (UN DESA, 2008, 2009). Such large urban agglomerations with more than 10 million inhabitants are commonly termed as "megacities", though this definition is rather loose (Molina and Molina, 2004). The rapid urbanization does not only pose logistical challenges to officials, also air quality control within such agglomerations is one major issue which needs to be addressed. Insufficient air quality e.g. is a threat to public health, affects regional ecosystems, and can have effects on regional climate (Molina and Molina, 2004). Since pollutants are also transported, influences can be expected not only on the megacities themselves, but also on a regional, continental, and global scale (Molina and Molina, 2004; Lawrence et al., 2007; Kunkel et al., 2012).

Therefore, the quantification of emissions from megacities and the assessment of the influences of these cities on their own air quality, but also on their surroundings are of major interest. Individual measurements of selected parameters, such as trace gases or chemical composition of aerosol particles, took place in several megacities, e.g. in Tokyo (e.g., Takegawa et al., 2006a; Xing et al., 2011), Beijing (e.g., Wang et al., 2010; van Pinxteren et al., 2009), New York City (e.g., Sun et al., 2011), or the Los Angeles basin (e.g., Hersey et al., 2011). In 2006, a large measurement campaign was conducted in the Mexico City Metropolitan Area: during the MILAGRO (Megacity Initiative: Local and Global Research Observations) field campaign, several stationary and mobile measurements were performed simultaneously to provide a comprehensive dataset of many atmospherically relevant parameters (Molina et al., 2010). However, Mexico City is very different from European megacities, such as Paris, in climatology (CONAGUA, 2011; Meteo France, 2011), topography and geographic properties, as well as emission patterns (Butler et al., 2008), and therefore results are not simply conferrable to Europe. One recent experiment in a major European metropolitan area took place in London in October 2006 and October/November 2007. These REPARTEE campaigns (Regents Park and Tower Environmental Experiment) were designed especially to provide measurements of horizontal and vertical fluxes within the city of London. Several trace gases as well as chemical and physical properties of aerosol particles were measured at various locations (Harrison et al., 2012). In Paris, so far several measurement campaigns were conducted with main focus on the gas phase (e.g., Gros et al., 2011; Menut et al., 2000; Vautard et al., 2003), or on particulate matter at one site within central Paris (e.g., Sciare et al., 2010; Widory et al., 2004). To provide a more comprehensive dataset of atmospheric measurements for this megacity, in July 2009 and January/February 2010, two large field campaigns were conducted in the Paris metropolitan area as part of the MEGAPOLI project (Megacities: Emissions, urban, regional, and Global Atmospheric POLlution and climate effects, and Integrated tools for assessment and mitigation). In both campaigns, three stationary measurement sites and several mobile platforms (airborne and ground-based) were employed, equipped with a suite of instruments to measure trace gas concentrations as well as chemical and physical properties of aerosol particles. This comprehensive dataset allows for a detailed characterization of physical and chemical processes within the Paris agglomeration and its pollution plume, and provides detailed observations as input for modelling purposes and for validation of model results.

Here, we present experimental results from the MEGAPOLI summer measurement campaign performed in Paris in July 2009, with the aim to characterize and quantify the impact of this European megacity onto its local air quality in comparison to the influence of regional, advected pollutants. We focus on the results of the measurements of the aerosol particle phase at the three stationary sites. The influence of air mass origin and meteorology on the measured aerosol particle mass concentration, chemical composition, and particle size distribution is discussed, with emphasis on the submicron size range. From the comparisons between the different sites, conclusions on the local and the regional contributions to measured concentrations of different chemical species are drawn. Furthermore, quasi-Lagrangian measurements during periods of connected flow conditions are investigated where one of the stationary sites was located downwind and one upwind of the city centre, allowing for a characterization of the impact of Paris' emissions onto local air quality. Complementary results from the wintertime campaign are presented in a companion paper (Crippa et al., 2013a).

2 Methods

2.1 Measurement sites and sampling

The MEGAPOLI summer measurement campaign took place in the greater Paris region during the whole month of July 2009. Here, we analyze data from measurements of volume mixing ratios of NO_x and O_3, of mass concentrations of submicron particulate sulphate, nitrate, ammonium, organics, and black carbon, and of particle size distributions in the size range from 4.9 nm to 10 µm for the time frame 30 June 2009, 18:00 until 31 July 2009, 15:50 (local time). Not all instruments were measuring during the whole period due to slightly different measurement time frames at the three sites and to down-times due to e.g. instrument calibrations, power failures, or instrumental problems. In the analysis, for averages over longer time periods therefore only data have been considered which cover at least 70 % of the respective time frame.

Measurement sites: three stationary measurement sites were operated during the MEGAPOLI campaign (Fig. 1). The first one was located at the LHVP (Laboratoire d'Hygiène de la Ville de Paris) in the centre of the city (13th district, 2°21′33.71″ E, 48°49′43.36″ N) (further referred to as the "Downtown" site). The LHVP building faces to a smaller street in the north-west and to a park in the south-east, and is about 400 m south-east from Place d'Italie, where seven large Parisian avenues are intersecting. This site is considered to represent Paris background air pollution (Sciare et al., 2010). The second station was located at a suburban site south-west from the city centre at SIRTA (Site Instrumental de Recherche par Télédétection Atmosphérique, 2°12′26.34″ E, 48°43′3.59″ N, Haeffelin et al., 2005) (further referred to as the "Suburban SW" site, abbreviated "Sub SW"). This measurement site was located on the grounds of the Ecole Polytechnique and is surrounded by fields to the west and north-west, and by villages in 1–3 km distance in the other directions. Major highways are located in about 3–6 km distance in all wind directions; a road with medium traffic is situated to the north in about 200 m distance. The third station was set up at a suburban site in the north-east of the centre of Paris at the Golf Départemental de la Poudrerie (http://poudrerie.ucpa.com/, 2°32′49.17″ E, 48°56′1.67″ N, further referred to as the "Suburban NE" site, abbreviated "Sub NE"). This measurement site, located at the periphery of a residential area on a small employee parking lot, was bordered to the north (from east to west) by a golf course and a forested park; to the south there was a road with medium traffic density in about 30 m distance. The two latter sites are considered to be representative for suburban sites influenced by local traffic emissions as well as the overall Paris emission plume. The three stationary sites were set up in a way that they provided connected flow conditions at SW and NE wind directions for quasi-Lagrangian measurements. The two suburban sites were located each in a distance of about 20 km from the Downtown site (see Fig. 1).

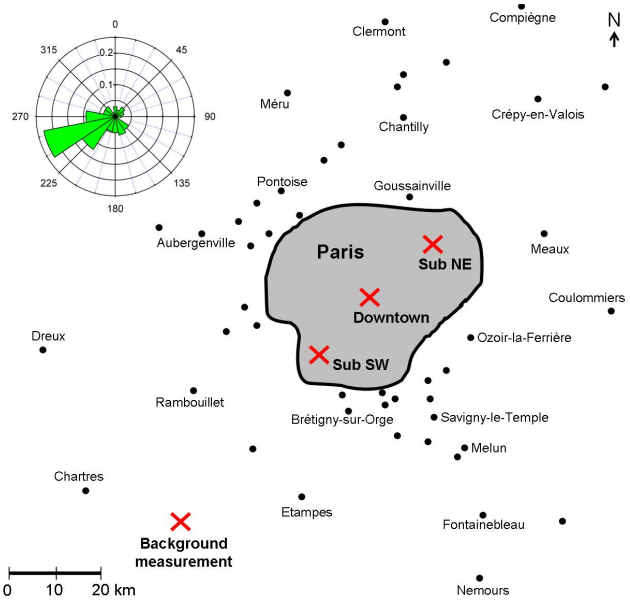

Fig. 1. Location of the stationary measurement sites (Downtown, Sub NE, Sub SW) and location of the short-time stationary background measurement during the campaign using the Mobile Laboratory (see Sect. 3.4). The Paris agglomeration is indicated as grey area; cities outside this agglomeration are denoted as black dots for better orientation. In the upper left, the relative distribution of wind directions observed at Sub NE during the whole campaign is shown.

Sampling techniques: at each measurement site, a suite of instruments was deployed for on- and off-line characterization of aerosol particle and gas phase as well as of meteorology. Here, only the sampling setups for the instruments used in the current analysis (Tables 1 and 2) are described.

At the *Downtown site*, gas analyzers as well as a TEOM-FDMS (tapered element oscillating microbalance – filter dynamics measurement system) and a PILS-IC (particle-into-liquid sampler coupled to an ion chromatograph) were sampling on the flat roof top of the LHVP building at about 14 m height above ground level. Both aerosol instruments were sampling through separate $PM_{2.5}$ cyclones (model SCC2.229, BGI Inc.). The PILS-IC was sampling through basic and acidic annular denuders (3-channel, URG Corp.), and daily filter measurements were performed to correct for background effects. The gas analyzers were located on the floor beneath the roof top and sampled via two independent 10 m long 1/4″ Teflon tubing sampling lines. A container was located next to the LHVP building, about 25 m south-east of the roof top sampling inlets, adjacent to a small park. Here, sampling was conducted at about 6 m a.g.l., and the inlet was equipped with a PM_{10} cyclone. This inlet was directly followed by an automatic drying system (Tuch et al., 2009) to keep relative humidity (RH) below 30 % at all times. MAAP

Table 1. Instrumentation for measurement of the particle phase used in this study.

Parameter(s)	Site	Instrument	Model (manufacturer)	Time resolution	Size range	Uncertainty estimate for comparisons[a]
Particulate organics, nitrate, sulphate, ammonium, chloride mass concentrations	Sub SW	HR-ToF-AMS	(Aerodyne Research, Inc.)	10 min[b]	~ PM_1 (lower size cut-off: ~ 70 nm)	30 % PMF results: 20 % PMF mass concentrations: 36 %
	Sub NE	C-ToF-AMS		1 min[c]		
	Downtown	HR-ToF-AMS		10 min[d]		
	MoLa[e]	HR-ToF-AMS		1 min[f]		
Black carbon mass concentration	Sub SW	Aethalometer	Model AE31[g] (Magee Scientific)	2 min	$PM_{2.5}$	30 %
	Sub NE	MAAP	Model 5012 (Thermo Scientific)	1 min	PM_1	10 %
	Downtown	MAAP		1 min	PM_{10}	
	MoLa	MAAP		1 min	PM_1	
Particle number concentration	Sub NE	CPC	Model 5403 (Grimm[h])	1 s	> 4.5 nm	
	MoLa	CPC	Model 3786 (TSI Inc.)	1 s	> 2.5 nm	
Particle number size distribution (d_{mob})	Sub SW	SMPS	Models 3080, 3081, and 3772[i] (TSI Inc.)	10 min	10.6–495.8 nm	
	Sub NE	EAS	(Airel Ltd.)	1 min	3.2 nm–10 µm[j]	
	MoLa	FMPS	Model 3091 (TSI Inc.)	1 s	5.6 nm–560 nm	
Particle number size distribution (d_o)	Sub NE	OPC	Model 1.109 (Grimm[h])	6 s	250 nm–32 µm	
	MoLa	OPC		6 s		
Particle number size distribution (d_{ca})	Sub NE	UV-APS	Model 3314 (TSI Inc.)	5 min	500 nm–15 µm[k]	
	MoLa	APS	Model 3321 (TSI Inc.)	1 s	500 nm–20 µm	
Total aerosol mass concentration	Sub NE	TEOM-FDMS	Models TEOM 1400a, FDMS 8500 (R&P[l])	15 min	PM_1	
	Downtown	TEOM-FDMS		6 min	$PM_{2.5}$	
Particulate sulphate mass concentration	Sub SW	PILS-IC[m]		8 min	$PM_{2.5}$	
	Sub NE	Quartz filters, off-line IC[n]		12 h	PM_1	
	Downtown	PILS-IC[m]		15 min	$PM_{2.5}$	

[a] See main text for definition of uncertainty estimate used here.
[b] Measurement cycle: 2.5 min each in V-mode ambient and thermodenuded, W-mode ambient and thermodenuded; MS/PToF cycles during V-mode: 10 s/10 s, W-mode: only MS, 10 s cycles.
[c] Measurement cycle: 20 s each in MS/PToF/LS mode.
[d] Measurement cycle: 5 min each in V-mode and W-mode; MS/PToF-cycles W-mode: only MS in 40 s cycles; V-mode: MS/PToF in 20 s/40 s cycles.
[e] Mobile Laboratory.
[f] Measurement cycle: V-mode, MS/PToF in 10 s/10 s cycles.
[g] 7-wavelength aethalometer.
[h] Grimm Aerosol Technik GmbH & Co. KG.
[i] Classifier model 3080, differential mobility analyzer model 3081, CPC model 3772.
[j] Only size range 4.86 - 486 nm used in the analysis (see text).
[k] Only channels from 750 nm onwards used (see text).
[l] Rupprecht & Patashnick Co., Inc.
[m] PILS (Orsini et al., 2003) coupled to an ion chromatograph (Dionex, model ICS2000) equipped with a 2 mm diameter auto-suppression, anion self-regenerating suppressor, a 2 mm diameter AS11-HC pre-column and column, and a 300 µL injection loop. For both PILS systems, liquid flowrates were delivered by peristaltic pumps set at 1.5 mL min^{-1} for producing steam inside the PILS, and at Sub SW at 0.25 mL min^{-1} for rinsing the impactor. At Downtown, a syringe pump was used at a flow of 0.8 mL min^{-1} for rinsing the impactor, here two ion chromatography systems (for cation and anion quantification) and a TOC (total organic carbon) system were connected to the PILS. For determination of anions, ion chromatography analysis was performed in isocratic mode at 12 mM of potassium hydroxide and a flowrate of 0.25 mL min^{-1}.
[n] 47 mm diameter pre-fired quartz filters (QMA, Whatman), analyzed using a 2 mm diameter AS11-HC model pre-column and column, a 20 µL injection loop, and an ion chromatograph (IC, model DX-600, DIONEX) equipped with a reagent free system (automated eluent generation and self-regenerating suppression).

(multi-angle absorption photometer) and AMS (aerosol mass spectrometer) (amongst other instruments) were connected to this main inlet via 3/4″ and 3 m of 1/8″ stainless steel tubing, respectively. Particle losses for the AMS sampling line were estimated using the Particle Loss Calculator (von der Weiden et al., 2009), and were found to be below 10 % for the relevant size range (0.1–1 µm; mean value: ~ 6 %).

At the *Suburban SW site*, several containers with measurement instruments were set up. AMS and SMPS (scanning mobility particle sizer), aethalometer and PILS-IC, and gas analyzers, respectively, were located in three separate containers. For AMS and SMPS, sampling occurred at about 4 m height a.g.l. through a PM_{10} inlet. The aerosol was dried using a Nafion drier and distributed via 6 mm stainless steel

Table 2. Instrumentation for measurements of gas phase and meteorological parameters used for this analysis.

Parameter(s)	Site	Instrument	Time resolution	Uncertainty estimate for comparisons[a]
NO_x	Sub SW	AC31M (NO)[b], NOxTOy (NO_2)[c,d]	1 min	20 %
	Sub NE	AirPointer[e]	1 min	
	Downtown	AC31M (NO_x)[b]	5 min	
	MoLa[f]	AirPointer[e]	1 min	
O_3	Sub SW	UV photometric O_3 analyzer[g]	1 min	10 %
	Sub NE	AirPointer[e]	1 min	
	Downtown	UV photometric O_3 analyzer[g]	5 min	
	MoLa	AirPointer[e]	1 min	
Temperature, RH, wind direction, wind speed	Sub NE	weather station[h]	1 min	
only Sub NE: solar radiation	MoLa	weather station[i]	1 min	
Mixed layer height	Sub SW	LIDAR[j]	1 h	

[a] See main text for definition of uncertainty estimate used here.
[b] AC31M, Environnement S.A. (detection of NO using ozone chemiluminescence; detection of NO_x using ozone chemiluminescence after thermal conversion to NO on molybdenum-converter).
[c] NOxTOy, METAIR (detection of NO_2 using chemiluminescence of luminol).
[d] NO_x was calculated from ($NO+NO_2$).
[e] AirPointer, recordum Messtechnik GmbH (UV photometric detection of O_3; detection of NO_x as under [b]).
[f] Mobile Laboratory.
[g] Model 49C, Thermo Environmental Instruments.
[h] Vantage Pro2, Davis Instruments.
[i] Vaisala.
[j] Wind Lidar Leosphere; mixed layer height retrieved using STRAT-2D algorithm (see text).

tubing to the instruments. The inlets for aethalometer and PILS-IC, located at 4 m a.g.l., were equipped with $PM_{2.5}$ cyclones (R&P and BGI Inc., respectively). The denuder system and the filter measurements for the PILS-IC were equal to those at the Downtown site. Gas analyzers were sampling via Teflon tubing from about 3.5 m height a.g.l.

At the *Suburban NE site*, all instruments were located in one container with an inlet at about 8 m above ground. The EAS (electrical aerosol spectrometer) was sampling directly from the main inlet. Insulated 1/2″ stainless steel tubing connected OPC (optical particle counter), UV-APS (ultraviolet aerodynamic particle sizer), MAAP, TEOM-FDMS, and filter sampler to the main inlet; 1/4″ tubing was used to connect the AMS and CPC (condensation particle counter). PM_1 cyclones were located directly in front of the MAAP, the TEOM-FDMS, and the filter sampler inlets, respectively. The aerosol sampled by OPC and UV-APS was dried using a silica gel diffusion drier. The sampling losses for this whole inlet system were calculated using the Particle Loss Calculator (von der Weiden et al., 2009), and were for all instruments below 10 % in their relevant measurement size range, with largest losses for smallest and largest particle sizes. Inlet losses for UV-APS and OPC for particle diameters larger than 5 µm were higher (approximately 30 % at 10 µm diameter). The weather station and the inlet to the 1/4″ Teflon sampling line for the gas analyzers were also located at the main inlet at about the same height as the aerosol inlet.

At the Suburban NE site, also the Mobile Laboratory MoLa (Drewnick et al., 2012) was stationed when not operating in the field, and measuring side by side to the stationary laboratory at about the same inlet height. The Mobile Laboratory was also measuring for one day each at both the Sub SW and the Downtown sites, respectively, for intercomparison purposes (Sect. 2.2). Furthermore, in Sect. 3.4 one selected stationary measurement of the Mobile Laboratory outside of Paris is used to complete the data base for the analysis.

2.2 Data acquisition and validation

The data acquisition of all instruments is described in Sect. 2.2.1, except for the AMS, which is treated in Sect. 2.2.2. As already mentioned, measurement data from the intercomparison periods (Sub NE: 274 h distributed over the whole campaign; Downtown: 17 July, 10:20–18:30; Sub SW: 23 July, 11:20–19:00) were used to compare the various instruments at the different sites to the instruments on-board the Mobile Laboratory. From these comparisons, estimates for the comparability of measurements from different sites have been deduced (see Tables 1 and 2). Note that these estimates do not reflect the uncertainty of the instruments or the measurements itself, but are solely used as a mean to ensure the comparability of measurements between the different sites. This also includes variations due to different sampling or working principles of the instruments. The results

of these intercomparisons are discussed in the following two sections.

2.2.1 Comparability of non-aerosol mass spectrometer measurements

Details on the instruments used (model and manufacturer) as well as on sampling intervals can be found in Tables 1 and 2, along with the estimated uncertainties of the associated measurements for comparison purposes. All intercomparison results are given in the Supplement in Tables S1 and S2 in detail. The main results are briefly summarized here.

Black carbon (BC) measurements from MAAPs at Sub NE, Downtown and the Mobile Laboratory showed good agreement (within 10 %). Differences in cut-offs did not seem to have a significant influence, confirming that BC is predominantly found in the submicron range (Seinfeld and Pandis, 2006). The aethalometer at Sub SW measured higher concentrations during the intercomparison period, compared to the MAAP on-board the Mobile Laboratory. We attribute this to instrumental differences which might limit the comparability with the MAAP measurements. Therefore, for the aethalometer, a larger uncertainty of 30 % is assumed here for comparison purposes.

Ozone (O_3) did show very good agreement in all intercomparisons (uncertainty estimated to 10 %). NO_x was measured using different techniques at the various sites (see Table 2). Despite this fact, at all sites the intercomparison measurements showed good agreement within an uncertainty of 20 %.

The OPC and CPC at Sub NE showed good agreement with the OPC and CPC on-board the Mobile Laboratory, respectively (within 10 and 30 %, respectively; the larger deviation for the CPC measurement is explainable by the differences in lower cut-offs of the instruments, see Table S2 for details). The UV-APS was only comparable (within 20 %) to the Mobile Laboratory APS for particles with continuum-aerodynamic diameter $d_{ca} \geq 750$ nm, likely due to slight instrumental differences. Therefore, only data for particle sizes from 750 nm onwards are used for the analysis. The size ranges of the EAS at Sub NE and the FMPS (fast mobility particle sizer) on-board the Mobile Laboratory overlap only between 4.86 and 486 nm (mobility diameter, d_{mob}). Therefore, comparison between the two instruments is only possible in this size range, and consequently only this size range has been used in the analysis. The comparison shows a mode in the number distribution measured by the FMPS around 10 to 15 nm which is likely an artefact due to the inversion algorithm used for this instrument (A. Wiedensohler, personal communication, 2012). The EAS does not show this mode, possibly due to differences in the analysis software used. However, no direct intercomparison measurements to SMPS systems were available for the EAS. Therefore, especially the smaller size mode (up to about 20 nm) has to be regarded with a higher uncertainty than the coarser size mode above 20 nm. For these larger particle sizes, the comparisons between FMPS and SMPS systems showed good agreement, and also the EAS and FMPS agree reasonably well (FMPS versus EAS number size distribution for sizes above 20 nm: slope $m = 0.80$, Pearson's $R^2 = 0.84$; total particle number concentrations agree within 15 % for particle sizes above 20 nm, else within 30 %). 12 h filter samples were taken on 47 mm quartz filters from which particulate sulphate was quantified using ion chromatography (IC); they were corrected from routinely taken blank filters. Meteorological data showed excellent agreement between the Mobile Laboratory and Sub NE. Furthermore, a comparison to wind data routinely measured at Sub SW showed little difference in the local wind speed and direction measured at the different sampling sites. Therefore, for the analysis, only meteorological data measured at Sub NE are used. The mixed layer height has been determined at Sub SW from routinely measured LIDAR (light detection and ranging) data using the STRAT-2D algorithm described in Haeffelin et al. (2012).

2.2.2 Aerodyne aerosol mass spectrometer measurements

At Sub NE, a C-ToF-AMS (compact time-of-flight aerosol mass spectrometer; Drewnick et al., 2005) was used, while at the other sites including the Mobile Laboratory, a HR-ToF-AMS (high-resolution ToF-AMS; DeCarlo et al., 2006) was deployed. These instruments were used to measure the submicron mass concentrations and size distributions of non-refractory particulate organic matter ("organics"), sulphate ("SO_4"), nitrate ("NO_3"), ammonium ("NH_4"), and chloride ("Chl"). All instruments measured at about 600 °C vaporizer temperature, only the Sub NE AMS was measuring at about 800 °C during the first two weeks of the campaign (30 June–14 July) to gather information concerning the dependency of organic fragmentation patterns on vaporizer temperature. However, no significant differences in organic fragmentation patterns or in mass concentrations due to heater temperature differences could be found in the semi-continuous intercomparison with the Mobile Laboratory AMS. Information on AMS measurement cycles can be found in Table 1. For the Downtown and the Sub SW site, we present only ambient MS (mass spectrum mode, yielding the average mass concentrations as described above) data acquired in V-mode, the lower resolution mode of the HR-ToF-AMS (as opposed to the higher resolution in W-mode). For the Sub NE site, only MS and PToF (particle time-of-flight mode, yielding the average mass size distributions) data are used. The C-ToF-AMS at the Sub NE site was additionally equipped with a light scattering probe (Cross et al., 2007), enabling single particle analysis. Results from this will be presented in an upcoming publication.

For all instruments, weekly calibration measurements of NH_4NO_3 particles (measurement in brute force single particle and MS mode; mobility diameter: 400 nm at Sub SW

and Downtown, 350 nm at Sub NE, and 550 nm in the Mobile Laboratory) to determine the AMS ionisation efficiency (IE), and measurements of filtered, particulate-free ambient air to correct for background effects have been performed throughout the campaign. A collection efficiency (CE) of 0.5 was assumed for all instruments as a typical value for fully neutralized, internally mixed particles with low to moderate nitrate content (Matthew et al., 2008). This CE was validated by comparisons with other instruments as described below. Standard relative ionisation efficiency (RIE) values (for SO_4: 1.2; organics: 1.4; NO_3: 1.1; NH_4: 4) were used if not noted otherwise below. The data analysis was performed with SQUIRREL (versions 1.48 to 1.51C, http://cires.colorado.edu/jimenez-group/ToFAMSResources/ToFSoftware/), applying the standard fragmentation table (Allan et al., 2004, with modifications according to Aiken et al., 2008, except for the Downtown site) with the respective individual corrections inferred from the measurements of particulate-free air.

Data validation for the different instruments: during the stationary measurements, the Mobile Laboratory AMS showed neutralized to slightly acidic aerosol within its measurement uncertainties. For 15 min averaged data, the linear fit through zero yielded a slope (m) of 1.32 and Pearson's R^2 of 0.97 for the correlation of measured ($NO_3^{molar} + 2\ SO_4^{molar} + Chl^{molar}$) versus NH_4^{molar}, with X^{molar} meaning the molar concentration of species X (Fig. S1a). For NH_4, a RIE of 4.1 was used, which was inferred from the NH_4NO_3 calibrations performed in MS mode. The total submicron particulate mass concentration measured by the Mobile Laboratory AMS plus the BC concentration measured by the MAAP on-board the Mobile Laboratory when parked at the Sub NE site agreed reasonably well with the total PM_1 mass concentration measured by the TEOM-FDMS at the same site ($m = 0.90$, $R^2 = 0.45$). Therefore, the AMS on board of the Mobile Laboratory seems well suited as reference instrument for the other AMSs.

For the AMS at Sub NE, laboratory calibration measurements of $(NH_4)_2SO_4$ were performed to determine the RIE of SO_4. This gave an RIE of 0.76. From the ammonium nitrate calibration measurements (MS mode) during the campaign, a RIE of 4.2 was estimated for NH_4. Using those RIE values, comparison of AMS SO_4 to filter measurements of particulate sulphate (using IC) showed satisfying agreement ($m = 1.18$, $R^2 = 0.72$), and the aerosol was found to be neutralized to slightly acidic ($m = 1.05$; $R^2 = 0.99$) (Fig. S1b). However, comparison to the Mobile Laboratory AMS showed significantly smaller organic mass concentrations for this instrument (Table S3). Direct comparison of the mass spectra of both instruments showed that this was likely due to the smaller ion transmission in the Sub NE AMS at larger mass to charge ratios (m/z's) compared to the Mobile Laboratory AMS, which is also the reason for the smaller RIE of SO_4 than typically used. Therefore, organics measured by the AMS at Sub NE were scaled with a factor of 1.5 (which would correspond to an effective RIE of organics of 0.93) to account for this effect. After this scaling, comparison of total mass concentration measured by MAAP and AMS with the total PM_1 mass concentration measured by TEOM-FDMS showed good agreement ($m = 0.94$, $R^2 = 0.74$) (Fig. S2).

At the Downtown site, due to a power failure during the night before the intercomparison measurement, the AMS was completely turned off, and only restarted directly before the intercomparison period (which therefore lasted only for ~ 5 h). Also, AMS measurements of particulate-free air could only be performed after the intercomparison, when the background already had decreased. Therefore, background values for the intercomparison period itself cannot be accounted for correctly. This affects especially NH_4, for which a large discrepancy in measured mass concentrations between the two instruments was found, while all other species agree within ~ 10 % (Table S3). The measured aerosol was neutralized to slightly acidic at this site throughout the campaign ($m = 1.18$, $R^2 = 0.99$) (Fig. S1c). Comparison of AMS SO_4 with sulphate mass concentrations from PILS-IC $PM_{2.5}$ measurements ($m = 0.95$, $R^2 = 0.76$) and of total particle mass concentrations from AMS and MAAP to TEOM-FDMS $PM_{2.5}$ ($m = 0.87$, $R^2 = 0.46$) showed reasonable agreement, especially when considering the different upper size cut-offs of the instruments.

For the AMS at the Sub SW site, a RIE for NH_4 of 3.3 was determined from the NH_4NO_3 measurements in MS mode. Still, comparison to the Mobile Laboratory AMS shows large discrepancies around 30 % for all species except for NH_4, for which the discrepancy is even larger (~ 70 %) (Table S3). These large and systematic negative differences of all species are likely due to large sampling losses, or to systematic errors in the IE calibration. Therefore, in order to be able to compare the measurements from the instruments of all sites, a general scaling of the Sub SW AMS to the Mobile Laboratory AMS measurements using a scaling factor of 1.3 for all species (see Table S3) was applied. After this scaling, comparison of SO_4 measured with the Sub SW AMS to sulphate from PILS-IC $PM_{2.5}$ measurements at the same site gives a more reasonable result ($m = 0.87$, $R^2 = 0.92$; before scaling: $m = 0.67$), despite differences in cut-offs. The aerosol measured with the Sub SW AMS was found to be neutralized to slightly acidic within the uncertainties throughout the whole campaign ($m = 1.29$, $R^2 = 0.99$) (Fig. S1d). However, no total aerosol mass concentration measurement was performed at this site, so only comparisons to total particle mass concentrations calculated from SMPS measurements are available. To convert mass concentrations into total particle volume concentrations, particles were assumed to be spherical and to exhibit a time-dependent density. The latter was inferred from the varying chemical composition and from densities of $1.72\,g\,cm^{-3}$ for NH_4NO_3, $1.77\,g\,cm^{-3}$ for $(NH)_2SO_4$, $1.5\,g\,cm^{-3}$ for organics, and $2\,g\,cm^{-3}$ for BC

(the average density of the whole campaign would correspond to 1.65 g cm^{-3}). The sum of calculated total particle volume from BC mass concentration and total mass concentrations measured with the AMS agrees reasonably well with the SMPS total particle volume concentration ($m = 0.93$, $R^2 = 0.54$; before scaling: $m = 0.74$, $R^2 = 0.56$) (Fig. S3). The upper size cut-off of the SMPS at about 500 nm (d_{mob}) corresponds to a vacuum-aerodynamic diameter of about 800 nm, which is similar to the cut-off for the BC and AMS measurements. All in all, these comparisons seem to validate the scaling procedure for the Sub SW AMS.

For all validated AMS measurements, a total uncertainty of 30 % is assumed, including uncertainties from RIE, IE, and CE determination. This is in line with typically observed uncertainties from instrumental comparisons of the AMS (Canagaratna et al., 2007).

2.3 Positive matrix factorization of AMS measurements

Positive matrix factorization (PMF; Paatero and Tapper, 1994) was applied to the time series of mass spectra of organics measured with the AMSs. PMF mathematically retrieves a given number of constant factor profiles (mass spectra in the case of AMS) and their contribution to the total measured mass spectrum for each time step by minimizing the residual between measured and modelled data, achieving both time series and mass spectra of a given number of factors without a priori information. To explore the possibility of different local minima, usually PMF solutions from a number of different randomly chosen starting points *("seeds")* are explored. Furthermore, the factor solutions derived by PMF are not unique, but (approximate) rotations of the matrices of factor time series and mass spectra may result in solutions which still meet the convergence criteria. This rotational ambiguity is explored by varying the so-called "*fpeak*" parameter. Details on application of PMF to AMS data can be found in (Ulbrich et al., 2009). The PMF Evaluation Tool (PET, version 2.03A) described by Ulbrich et al. (2009) was used in this analysis using the PMF2 algorithm (Paatero, 1997). For the three AMS datasets, matrices with the time series of the organics mass spectra and the associated errors were retrieved from SQUIRREL using the standard fragmentation table (Allan et al., 2004). Details on the data matrix treatment for preparation for PMF and on the PMF analysis itself can be found in Table S4. From all datasets, individual extraordinarily high data points ("spikes") in the data and error matrices, which could not be fitted appropriately by the algorithm, were removed iteratively. From the Sub NE dataset, furthermore two time periods of a few hours each were removed which were measured during nearby fireworks on the night before 14 July, and during residential trash burning in the neighbourhood on 11 July to avoid artificial biases of the PMF analysis. For further validation of the method, for the Sub NE dataset, PMF was performed both on the whole dataset and for the periods with higher and lower heater temperature separately, however, no significant differences were found. Therefore, only the PMF solutions using the whole dataset were evaluated further and are presented here. For all datasets, the pre-defined number of factors to be calculated by PMF was varied from 1 to 5 with a "coarse" variation of *fpeak* parameters (see Table S4). The two-factor solution was found to explain best the data from the Sub NE and the Sub SW site, while for the Downtown site, both the two- as well as the three-factor solution were found suitable. These results are discussed in more detail in Sect. 3.1. For the Sub SW and Downtown site, the solutions with more factors showed splitting of the factors, which after inspection of mass spectra and time series were identified as physically meaningless. For the Sub NE site, the third factor obtained in the three-factor solution was driven by instrumental noise and could not be suppressed by any data pre-treatment. This factor was still present also at higher factor solutions (solutions with more factors). Furthermore, these higher factor solutions resulted again in a physically meaningless splitting of the other factors. Therefore, only the two-factor solution was used for further analysis. In all cases, also *fpeak* and *seed* variations did not provide more reasonable results for higher factor solutions. Time series and mass spectra of higher factor solutions for the different sites are shown in the Supplement (Figs. S4 to S6).

For the chosen number of factors, *fpeak*s were varied in steps of 0.1 from -1.5 to 1.5. There was no indication that any other solution than those with *fpeak* $= 0$ might provide physically more meaningful results. Therefore, *fpeak* $= 0$ was used for the further analysis. In addition, *seeds* were varied from 0 to 50 in steps of 1 for the chosen solutions at *fpeak* $= 0$. No differences in the solutions at varying *seeds* were found for the chosen solutions with exception of the three-factor solution at the Downtown site, where 2 out of 51 solutions gave slightly different results, but with very similar time series and mass spectra as for the other solutions. Therefore, only the *seed* $= 0$ solutions were regarded further. However, the variation of the results upon varying *fpeak*s and *seeds* were used as a measure of the uncertainty of the chosen PMF solutions, both for the obtained factor mass spectra and the time series. To calculate these uncertainties, for each data point (m/z or time step, respectively) the average and the standard deviation of all solutions was calculated. To calculate the relative uncertainty of the mass spectra (Δ_{MS}), the sum of the absolute standard deviations for the individual m/z's was calculated and divided by the sum of the signal of the average mass spectrum (Eq. 1). For calculation of the relative uncertainty of the factor time series (Δ_{TS}) according to Eq. (2), the time series of the absolute standard deviations was divided by the average time series to give the relative standard deviation of each data point. The average of these relative standard deviations gave the overall uncertainty of the time series.

$$\Delta_{\mathrm{MS}} = \frac{\sum_{i=1}^{n} \sigma_{\mathrm{p},i}}{\sum_{i=1}^{n} \bar{x}_{\mathrm{p},i}} \quad (1)$$

$$\Delta_{\mathrm{TS}} = \frac{\sum_{i=1}^{n} \frac{\sigma_{\mathrm{p},i}}{\bar{x}_{\mathrm{p},i}}}{n} \quad (2)$$

n: the number of m/z's or time steps, respectively; $\bar{x}_{\mathrm{p},i}$: the average for one m/z or time step; $\sigma_{\mathrm{p},i}$: the standard deviation for one m/z or time step.

The calculated uncertainties for all PMF results can be found in Table S5. In general, the uncertainties from *seed* variations are much smaller than those from *fpeak* variations (e.g., for the two-factor solutions, uncertainties from *seed* variations are around 1 %, while *fpeak* variation usually gives uncertainties of the order of 10–20 %), indicating that the solutions are relatively stable independent of the chosen *seed*. Relative uncertainties of time series are usually slightly larger than those of the mass spectra, but of the same order of magnitude. All estimated uncertainties (from *fpeak* and *seed*) for the two-factor solutions from the different sites are below about 20 %. The uncertainties for the Downtown three-factor solution are larger, especially for the two different HOA (hydrocarbon-like organic aerosol) factors (up to about 40 %). This reflects the associated uncertainty in the retrieval of factors related to different sources (and therefore, with different time series), but with very similar mass spectra.

As discussed in Sect. 3.1, only the two-factor solutions from all sites are used for the following study. From the estimated uncertainties given in Table S5, an upper limit of uncertainty at about 20 % for these two-factor solutions can be deduced. This uncertainty of the PMF analysis, together with the uncertainty of the AMS measurement itself (30 %), results in a total uncertainty for the absolute mass concentrations of the individual organic aerosol types from the PMF solutions of $((30\,\%)^2 + (20\,\%)^2)^{1/2} = 36\,\%$.

PMF solutions of the AMS measurements in the Mobile Laboratory as described in von der Weiden-Reinmüller et al. (2013) are also used in the following analysis. Those results are described in Sect. 3.1.

2.4 Particle dispersion model FLEXPART

The Lagrangian particle dispersion model FLEXPART (Stohl et al., 2005), version 8.2, was used to assess the origin of air masses sampled at the stationary sites. 20-day backward simulations were performed for the Sub NE site at 3 h time resolution using ECMWF (European Centre for Medium-Range Weather Forecasts) meteorological data by releasing 60 000 particles at the measurement location and following them backward in time. In this analysis, for the determination of air mass origin, *footprint emission sensitivities* for aerosol tracers were used. The so-called *emission sensitivity* is proportional to the residence time of the particles over a given grid cell, while the *footprint emission sensitivity* represents this *emission sensitivity* integrated over the lowest 100 m of the atmosphere. The *footprint emission sensitivity* therefore gives an indication where emissions could have been taken up effectively by the air mass that arrived at a certain time at the measurement site. Multiplying the *footprint emission sensitivity* with emission fluxes from a spatially disaggregated inventory gives the distribution of emissions contributing to the simulated mixing ratio at the receptor site. Removal processes for aerosol particles (wet and dry deposition) are also taken into account in the simulations.

Furthermore, for each 3 h data point, the integral of *footprint emission sensitivity* over the total land surface area has been calculated. This integral gives the absolute continental contribution to the *footprint emission sensitivity* for a given air mass, and therefore gives an indication for the amount of continental influence on the sampled air masses.

3 Results and discussion

3.1 Identification of the PMF factors

Correlations of the time series of the PMF factors found for the different sites (as described in Sect. 2.3) with time series of external tracers, measured at the respective site (SO_4, NO_3 from AMS measurements, and BC and NO_x) are presented in Table S6. Correlations of the factor mass spectra with reference mass spectra from the literature are shown in Table S7.

For the two-factor solutions, time series of factor 1 of the three sampling sites correlate better with time series of primary emission tracers (NO_x and BC, Pearson's R^2 usually on the order of 0.2 to 0.3) than with that of secondary species (SO_4 and NO_3, R^2 usually below 0.1). The respective mass spectra correlate very well (Pearson's R^2 typically about 0.8) with reference mass spectra of HOA (hydrocarbon-like organic aerosol; Ulbrich et al., 2009) and cooking-related organic aerosol (Allan et al., 2010; He et al., 2010), which both are related to primary emissions. Time series of factor 2 of all three sampling sites correlate with time series of secondary species (SO_4 and NO_3, R^2 typically around 0.5 and 0.2–0.3, respectively), and the respective mass spectra correlate very well with low-volatile OOA (low-volatile oxygenated organic aerosol, R^2 about 0.9) and to a lesser extent also with semi-volatile OOA (semi-volatile oxygenated organic aerosol, R^2 about 0.6 to 0.7) (both from Ulbrich et al., 2009). Therefore, we classify factor 1 of all three sampling sites as comparably fresh "HOA", while factor 2 is identified as more aged "OOA". These classifications are summarized in Table S6.

The correlations of the OOA factor time series are generally better with SO_4 mass concentration time series than with those of the semi-volatile NO_3. Furthermore, the retrieved factor mass spectra do resemble more low-volatile OOA than semi-volatile OOA reference mass spectra (Table S7). Both observations point to the fact that the retrieved OOA factors are dominated by low-volatile rather than semi-volatile organic compounds. Semi-volatile OOA is thought of as having an oxidation state between HOA and low-volatile OOA (Jimenez et al., 2009); therefore it is not surprising that mass spectra of the retrieved HOA and OOA classes do correlate with the reference mass spectrum of semi-volatile OOA similarly (R^2 about 0.5 to 0.7), but neither exceptionally well.

The correlations of the HOA factor time series with the primary emission tracer time series are better than those with secondary species, but still rather low (R^2 usually about 0.2 to 0.3). For the Downtown site, the HOA factor can be split up into two HOA-like factors when moving from the two- to a three-factor solution (Fig. S5). From these factors, one factor (factor 3) correlates much better with the primary emission tracer time series (R^2 about 0.5 to 0.7), while the other (factor 1) correlates much worse ($R^2 < 0.2$). In addition, factor 3 shows a much better similarity with HOA reference mass spectra than the HOA from the two-factor solution. Since HOA usually is associated with emissions from traffic (e.g., Zhang et al., 2011), as are also the primary emission tracers NO_x and BC, this all together indicates that factor 3 represents a part of the total HOA from the two-factor solution which is likely traffic-related.

Figure 2 shows the diurnal cycles of all HOA-like factors retrieved for the Downtown site with the different PMF solutions. The more traffic-related HOA-like factor ($HOA_{traffic\_rel.}$) from the three-factor solution peaks during the morning and the evening hours, consistent with rush hour times. The other HOA-like factor from the three-factor solution shows a peak during the evening and around noon, when no peaks in NO_x and BC are observed (Fig. 5a). Such a diurnal pattern for a HOA-like PMF factor was also observed e.g. by Allan et al. (2010) in Manchester and London and attributed to cooking-related primary emissions. Similar to our findings, also Allan et al. (2010) found only a weak correlation of the time series of this factor with that of BC. The interpretation of this factor (factor 1 of the three-factor solution) as "cooking-related organic aerosol" ($HOA_{cooking\_rel.}$) would be reasonable since the Downtown measurement site was situated in an area where several restaurants are located. However, comparison with reference mass spectra proves difficult, as the mass spectra found for traffic- and cooking-related emission sources are very similar. Both the mass spectra of our more traffic-related HOA factor as well as the apparently more cooking-related HOA factor correlate well ($R^2 > 0.8$) with the cooking-related organic aerosol factors found by Allan et al. (2010); however, contrary to expectations, our $HOA_{cooking\_rel.}$ factor correlates worse ($R^2 = 0.64$) with cooking-related organic aerosol source spectra

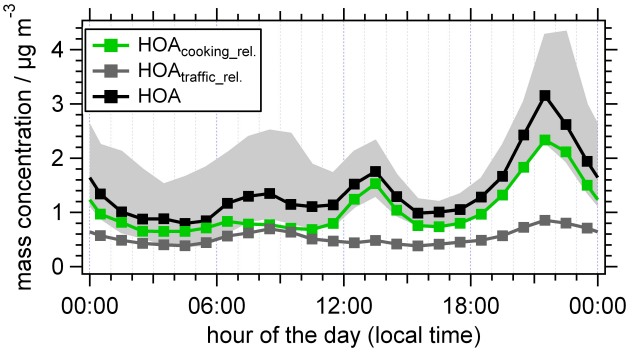

Fig. 2. Diurnal pattern (hourly median values for the whole campaign) of HOA from the two-factor solution, and the two HOA-like factors ($HOA_{traffic\_rel.}$, $HOA_{cooking\_rel.}$) from the three-factor solution retrieved for the Downtown site. Percentiles (25 and 75 %, light grey shading) are only shown for HOA from the two-factor solution for clarity.

published by He et al. (2010) than the $HOA_{traffic\_rel.}$ factor ($R^2 = 0.80$). Thus, further work is needed to characterize varying cooking sources and get a more comprehensive dataset of mass spectra and typical mass spectral markers characteristic for ambient, cooking-related organic aerosol. The diurnal pattern of the HOA especially from the Sub NE site is similar to that of the Downtown site two-factor solution HOA (Fig. S7). Therefore, it cannot be excluded that also the HOA factors of the suburban sites contain a contribution from cooking-related organic aerosol. This would also explain the low correlations of the HOA factors with NO_x and BC for these two sites. However, due to the mass spectral similarity of $HOA_{traffic\_rel.}$ and $HOA_{cooking\_rel.}$, this separation of the two HOA factors cannot be achieved for the Sub SW and Sub NE site, which are not located in a region with as many cooking-related sources nearby as the Downtown site.

For Sub SW, the two aforementioned HOA factors can be distinguished via PMF of the high resolution mass spectra (Crippa et al., 2013b). However, within the framework of this paper, where we compare measurements at the three different stationary sites, only the two-factor solutions from PMF of unit mass resolution mass spectra are used for all sites for better comparability. As both, traffic- as well as cooking-related emissions, are generated by local primary emissions opposed to more aged secondary species within the OOA factor, and since this is the main information needed for the following analysis, this mixture of different sources within a single factor is no drawback.

For the Mobile Laboratory AMS measurements during this campaign, von der Weiden-Reinmüller et al. (2013) were able to identify a physically meaningful four- and a five-factor solution from the PMF analysis. In the four-factor solution, one traffic-related HOA-like factor ($HOA_{traffic\_rel.}$), one cooking-related HOA-like factor ($HOA_{cooking\_rel.}$), one

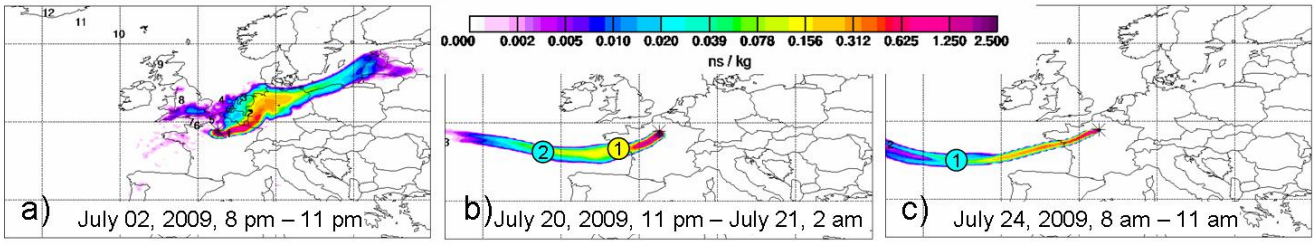

Fig. 3. Examples for **(a)** "Central Europe", **(b)** "Atlantic Polluted", and **(c)** "Atlantic Clean" air masses distinguished using FLEXPART *footprint emission sensitivities*. The numbers in circles denote the approximate location of the centroid of the air mass at the respective number of days prior to sampling.

semi-volatile OOA-like factor, and one low-volatile OOA-like factor were retrieved. The first three factors were found to be associated with the Paris emission plume. In the five factor solution, one more semi-volatile OOA-like factor was retrieved, which originates from both the low-volatile OOA-like and the three plume-related factors from the four-factor solution. For the four-factor solution, from the long-term intercomparison measurements at the Sub NE site, it was found that low-volatile OOA retrieved from the Mobile Laboratory AMS data corresponds to the OOA retrieved from the Sub NE site data (Pearson's R^2 for linear correlation of time series: 0.91; for mass spectra: 0.99), while the sum of $HOA_{traffic\_rel.}$, $HOA_{cooking\_rel.}$ and the semi-volatile OOA-like factors of the Mobile Laboratory AMS (this sum further referred to as "HOA" for the Mobile Laboratory) corresponds to the HOA retrieved at the Sub NE site (R^2 for time series: 0.81; for mass spectra: 0.90). From the intercomparison measurements at all stationary sites, good correlations between the OOA and the HOA factor time series of the Mobile Laboratory and the respective sites are found (Table S8), with a deviation within the uncertainty of 20 % which was calculated for the PMF factors in Sect. 2.3. Also the mass spectra (Fig. S8) exhibit the same features for each organic aerosol type at all sites. For the five-factor solution, the "new" semi-volatile OOA cannot be assigned clearly to either the OOA or the HOA from the stationary sites. Therefore, in the following analysis, HOA and OOA from the two-factor solutions for the stationary sites, and the corresponding OOA and combined HOA-like factors from the four-factor PMF solution for the Mobile Laboratory (combined as described above) are compared to each other within the associated uncertainty discussed in Sect. 2.3.

3.2 Classification of air masses

The air masses sampled at the stationary sites were classified using the output of the FLEXPART simulations described in Sect. 2.4. Three major classes of air masses were distinguished: "Central Europe", "Atlantic Clean", and "Atlantic Polluted".

Only during the first days of the field campaign, air masses from eastern continental Europe were advected; an example is shown in Fig. 3a. These air masses, which had travelled for several days over polluted continental regions, were classified as "Central Europe" air masses. For the remaining time of the campaign, air masses were mostly advected from south-westerly to north-westerly directions, namely from the Atlantic Ocean, passing western France on different routes. They were classified as "Atlantic Clean" or "Atlantic Polluted" air masses, depending on their residence time over continental areas. This residence time was estimated using the location of the centroid of the air mass 24 h prior to sampling (provided from the FLEXPART simulations, denoted with a circled "1" in Fig. 3b and c). Air masses which were travelling rather fast (which means, the centroid of the air mass was far outside the French west coast one day prior to sampling; this corresponds to a travelling velocity of the air mass of approximately 1200 km per day, i.e. an average transport velocity of $\sim 14\,m\,s^{-1}$) were regarded as "Atlantic Clean", as they did not have a long residence time over continental areas (Fig. 3c) before arriving at the Paris metropolitan area. Air masses at the coast or over land one day prior to sampling were classified as "Atlantic Polluted" (Fig. 3b), unless removal processes especially via precipitation had taken place during the last two days of the travelling time of the air mass before arrival at the sampling sites, in which case they were classified as "Atlantic Clean". Furthermore classified as "Atlantic Polluted" were air masses which had remained for a longer period of time over Spain and the heavily anthropogenically influenced region in the Atlantic Ocean between Spain and France.

The resulting time series of various aerosol components, measured with the AMSs at the three stationary sites, together with the air mass classification are shown in Fig. 4. The uppermost panel of Fig. 4 shows the time series of the absolute continental contribution to the *footprint emission sensitivity* of the sampled air masses as calculated from FLEXPART (see Sect. 2.4). In total, 62 h of "Central Europe", 257 h of "Atlantic Polluted", and 423 h of "Atlantic Clean" air masses were sampled during the whole

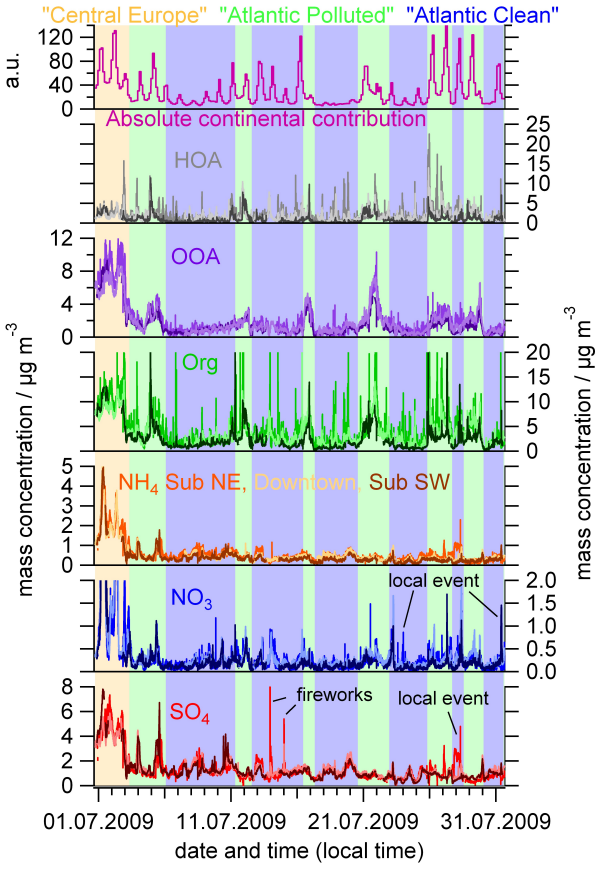

Fig. 4. Classification of the sampled air masses (orange, green, and blue background for "Central Europe", "Atlantic Polluted", and "Atlantic Clean" air masses, respectively), time series of calculated absolute continental contribution to *footprint emission sensitivity*, and selected species (SO_4, NO_3, NH_4, organics, and OOA and HOA retrieved from total organics using PMF) measured with the AMS at the three stationary sites (Sub NE: medium coloured, Downtown: light coloured, Sub SW: dark coloured curves). Some local events at single sites in the time series of NO_3 and SO_4 as discussed in Sect. 3.3.1 are marked.

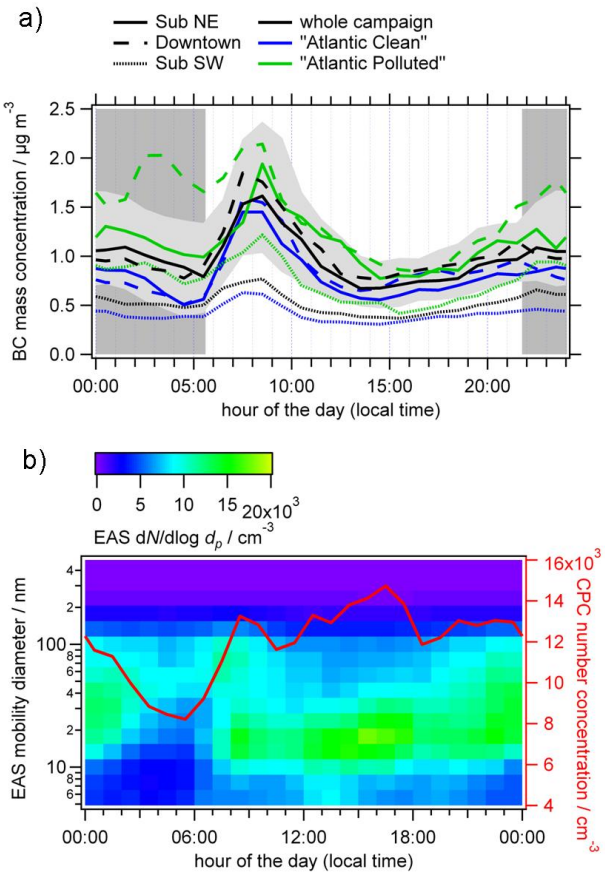

Fig. 5. (a) Diurnal cycles (hourly median values) of BC mass concentration at the three stationary sites (for the whole campaign, and for "Atlantic Polluted" and "Atlantic Clean" air masses separately). Percentiles (25 and 75 %) are shown exemplarily in light grey for the measurement at Sub NE (whole campaign); all other percentiles are omitted for clarity. The time period between sunset and sunrise is shaded in grey. **(b)** Diurnal cycles (hourly median values) of EAS number size distribution and CPC number concentration measured at the Sub NE site.

measurement period. A discussion of the characteristics of the different types of air masses is given in the next section.

3.3 Influence of air mass origin and meteorology

3.3.1 Averages and diurnal cycles

Averages of selected meteorological, gas phase and particle phase parameters for the different sites and air masses are given in Table 3. The origin of air mass was similar for both "Atlantic" air masses, which is also reflected in the average wind directions (south to south-west for the "Atlantic" air masses, north-east for "Central Europe" air masses). On the other hand, meteorological parameters such as average temperature and wind speed were more similar between "Central Europe" and "Atlantic Polluted" air masses. Temperature was lower and wind speed was higher on average for the "Atlantic Clean" air masses. Since, by definition, the relevant difference of the "Atlantic Clean" air masses from the "Atlantic Polluted" air masses is the shorter residence time over land, this higher average wind speed associated with the former air masses is not surprising. The differences in residence time over land for all three air mass categories are also evident in the continental contribution to the *footprint emission sensitivity*, which from the FLEXPART calculations was found to be highest for "Central Europe" air masses, and lowest for the "Atlantic Clean" air masses.

Primary emission tracers: at all sites, the diurnal cycles of the primary emission tracers BC (Fig. 5a), HOA (Figs. 2 and S7), and NO_x (not shown; the diurnal cycle is comparable to that of BC) show peaks during the morning and the evening rush hours, consistent with their association with

Table 3. Meteorological parameters measured at and modelled for Sub NE; gas phase parameters and particle chemical composition measured at the respective sites. Given are the averages with uncertainty ranges as deduced in Sect. 2, except for meteorological parameters, where means and standard deviations are provided. Chloride as measured by the AMS was below 0.1 $\mu g\,m^{-3}$ at all sites for all averages and was therefore not regarded for this analysis.

Meteorology					
Air mass	Temperature/ °C	Relative humidity/%	Wind speed /m s^{-1}	Wind direction	Continental contribution/ ns kg^{-1}
"Central Europe"	24 ± 4	64 ± 15	1.3 ± 1.1	23.7 °	62 ± 30
"Atlantic Polluted"	22 ± 4	57 ± 17	1.4 ± 1.3	189.1 °	34 ± 28
"Atlantic Clean"	18 ± 3	63 ± 15	2.2 ± 1.6	243.2 °	20 ± 21

Gas phase parameters						
	NO_x/ppb			O_3/ppb		
Air mass	Sub NE	Downtown	Sub SW	Sub NE	Downtown	Sub SW
"Central Europe"	11 ± 2	21 ± 4	–	51 ± 5	60 ± 6	–
"Atlantic Polluted"	10 ± 2	20 ± 4	9 ± 2	32 ± 3	29 ± 3	33 ± 3
"Atlantic Clean"	11 ± 2	15 ± 3	6 ± 1	25 ± 3	25 ± 3	26 ± 3
Particle phase chemistry						
	BC/$\mu g\,m^{-3}$			HOA/$\mu g\,m^{-3}$		
Air mass	Sub NE	Downtown	Sub SW	Sub NE	Downtown	Sub SW
"Central Europe"	1.7 ± 0.2	2.3 ± 0.2	–	2.5 ± 0.9	2.1 ± 0.8	–
"Atlantic Polluted"	1.2 ± 0.1	1.7 ± 0.2	0.8 ± 0.2	2.2 ± 0.8	2.4 ± 0.9	1.5 ± 0.5
"Atlantic Clean"	1.0 ± 0.1	1.0 ± 0.1	0.6 ± 0.2	1.2 ± 0.4	1.3 ± 0.5	0.5 ± 0.2
	SO_4/$\mu g\,m^{-3}$			OOA/$\mu g\,m^{-3}$		
Air mass	Sub NE	Downtown	Sub SW	Sub NE	Downtown	Sub SW
"Central Europe"	4.2 ± 1.3	3.8 ± 1.1	–	7.7 ± 2.8	6.0 ± 2.2	–
"Atlantic Polluted"	0.9 ± 0.3	1.1 ± 0.3	1.1 ± 0.3	2.4 ± 0.9	2.5 ± 0.9	1.8 ± 0.6
"Atlantic Clean"	1.1 ± 0.3	1.2 ± 0.4	1.0 ± 0.3	0.9 ± 0.3	0.9 ± 0.3	0.7 ± 0.3
	NO_3/$\mu g\,m^{-3}$			NH_4/$\mu g\,m^{-3}$		
Air mass	Sub NE	Downtown	Sub SW	Sub NE	Downtown	Sub SW
"Central Europe"	2.1 ± 0.6	2.4 ± 0.7	–	2.1 ± 0.6	1.9 ± 0.6	–
"Atlantic Polluted"	0.2 ± 0.1	0.3 ± 0.1	0.2 ± 0.1	0.4 ± 0.1	0.4 ± 0.1	0.3 ± 0.1
"Atlantic Clean"	0.2 ± 0.1	0.2 ± 0.1	0.1 ± 0.03	0.5 ± 0.2	0.4 ± 0.1	0.3 ± 0.1

traffic emissions. The HOA diurnal cycles furthermore exhibit a peak around noon due to additional primary emission sources, such as cooking, as discussed in Sect. 3.1. The mixed layer height begins to rise in the morning starting with sunrise at about 05:30, and reaches its maximum at around 18:30. After that it declines and reaches its lowest value around 20:00 (slightly before sunset), and remains constant at this level throughout the night (Fig. S9). Therefore, the observed maximum of primary emission tracer concentrations in the morning at around 08:00–09:00 cannot be solely induced by the breaking up of the boundary layer, but also is caused by the temporal variation of local emission strengths. As those peaks occur simultaneously at all three stationary sites, and show no delay in time relative to each other, local emissions of HOA, BC, and NO_x seem to be present within the whole Paris area, and emissions close to the measurement stations seem to be dominating also at the suburban sites. The effect of advected primary emissions of these tracers from the greater Paris area (the latter being referred to as the "Paris emission plume" within the context of this work) was only found to make a minor contribution to primary emission tracer concentrations at the suburban sites, as discussed in Sect. 3.5.

For both types of "Atlantic" air masses, diurnal cycles of primary emission tracers show comparable shapes for all three sites. Differences are only observed in the absolute values reached, which is also reflected in the averages of NO_x volume mixing ratio, and HOA and BC mass concentrations for the different air masses as shown in Table 3. At a given site, generally those averages are similar

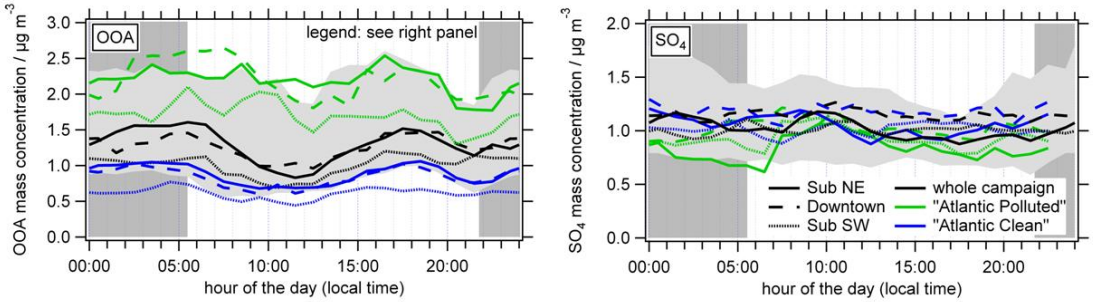

Fig. 6. Diurnal cycles (hourly median values) for OOA (left) and SO_4 (right) at all sites for the whole campaign, and for "Atlantic Polluted" and "Atlantic Clean" air masses separately. The time period between sunset and sunrise is shaded in grey. Percentiles (25 and 75 %) are shown in light grey exemplarily for the measurements at Sub NE only (whole campaign).

for "Central Europe" and "Atlantic Polluted" air masses, but lower for "Atlantic Clean" air masses. This is especially visible at the Downtown site, while at Sub NE, this is observable only for some species (especially HOA). For Sub SW, no averages for "Central Europe" air masses are available due to instrumental downtimes. These differences of the primary emission tracer concentrations for the different air masses cannot be due to air mass origin or spatial distribution of local sources, since then rather the two "Atlantic" air masses would show similar concentrations of primary emission tracers than "Central Europe" and "Atlantic Polluted". This behaviour can rather be explained by the higher average wind speed which was observed during the "Atlantic Clean" air masses, which leads to a larger dilution of primary emissions and consequently to lower concentrations of the associated tracers compared to the situation for the other two air masses. Therefore, in our case, wind speed seems to be the dominating factor for the averages of primary emission tracers observed at a given site.

For a given air mass, average concentrations of primary emission tracers generally are different for the three measurement sites. This is due to the different exposure of the sites to primary emissions, as described above, and in addition due to the different influences of advected emissions from the whole agglomeration, as discussed in Sect. 3.5. In contrast, for secondary species OOA, SO_4, NO_3, and NH_4, within the uncertainties the same average mass concentrations are observed at all sites for a given type of air mass. A similar distribution is found for O_3. This seems to indicate a more regionally homogeneous distribution of these secondary species over the greater Paris region, rather than a distribution dominated by local production. This conclusion is backed up by a background measurement case study using the Mobile Laboratory, which is presented in Sect. 3.4.

Inorganic species: at all sites, comparable average mass concentrations for inorganic species (SO_4, NO_3, NH_4) were measured during both "Atlantic" air masses, but much higher mass concentrations were found when "Central Europe" air masses were advected. Here, origin of air mass rather than local conditions seems to be the dominating factor that determines the pollutant concentrations. The regional character of SO_4 is also reflected in its diurnal cycle (Fig. 6), which shows no or only a very small diurnal trend for any of the sites and air masses. This lack of differences between the two types of "Atlantic" air masses in SO_4 diurnal cycles and average mass concentrations indicates that the relatively short residence times over land for both of these air masses are (in the absence of cloud processing) not sufficiently long to generate SO_4 from precursor gases that were picked up (Seinfeld and Pandis, 2006). This is also supported by the fact that the measured average SO_4 mass concentrations for "Atlantic" air masses of about 1 µg m^{-3} are typical for anthropogenically influenced marine air masses without significant continental influence, as it was measured with the AMS in several European coastal regions. For example, SO_4 mass concentrations of 1.15 µg m^{-3} for continental marine aerosol were measured in early summer 2008 at Mace Head (Dall'Osto et al., 2010a, b), and 0.91 µg m^{-3} of SO_4 were measured for marine aerosol in late autumn 2008 at the southern coast of Spain (Diesch et al., 2012). This aerosol is not necessarily of biogenic origin, as for pristine regions, much lower particulate sulphate mass concentrations have been reported, e.g., 0.18 µg m^{-3} in clean South Atlantic regions (Zorn et al., 2008). Therefore, a large extent of this aerosol is likely due to e.g. ship emissions and other anthropogenic sources.

The diurnal cycle of NO_3, on the other hand, is driven both by the temperature and RH dependence of the gas-particle-partitioning of NH_4NO_3 (Fig. 7). Again, average mass concentrations are much higher for the "Central Europe" air masses than for the "Atlantic" air masses. Differences in mass concentrations between the two "Atlantic" air masses would be much more likely to expect for NO_3 than for SO_4, as NO_3 forms much faster from precursor gases (Seinfeld and Pandis, 2006). However, due to the very low measured mass concentrations, no significant differences can be found between the two types of air masses. The same holds for O_3 and for NH_4, which neutralizes SO_4 and NO_3 almost fully during the whole campaign (see also Sect. 2.2.2).

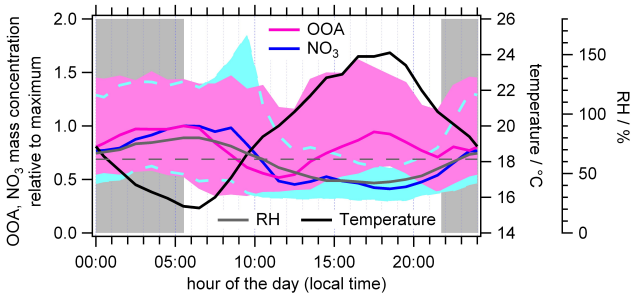

Fig. 7. Diurnal cycles (hourly median values) for the whole measurement campaign for the temperature and RH, and diurnal cycles for NO_3 and OOA, normalized to their respective maxima, all measured at Sub NE. Percentiles (25 and 75 %) are shown in light pink for OOA, and in light blue for NO_3. The time period between sunset and sunrise is shaded in grey. Deliquescence RH for NH_4NO_3 of 62 % (for 20 °C; Seinfeld and Pandis, 2006) for the transition of the solid to the liquid phase is marked as a dashed horizontal line.

In summer 2010, PM_1 measurements with an AMS were performed at a research station at the Puy de Dôme (1465 m altitude) in south-central France (Freney et al., 2011). During this campaign, air mass origin most of the time was similar to air masses classified as "Central Europe" in the present study. Freney et al. (2011) found average mass concentrations of 5.45 µg m^{-3} of SO_4, compared to 4.2 ± 1.3 µg m^{-3} (measured at Sub NE during "Central Europe" air masses) in this study. NO_3 was even better comparable (2.33 µg m^{-3} compared to 2.1 ± 0.6 µg m^{-3} as found in the present study). Therefore, inorganic mass concentrations measured during this campaign during "Central Europe" air masses seem to be common for such types of air masses, at least in summertime.

The influence of air mass origin on inorganic species mass concentrations measured in Paris was also found by Sciare et al. (2010) in a previous study. During this measurement campaign in May/June 2007, the total ion mass concentration in $PM_{2.5}$ was found to be much higher for air masses advected from continental Europe than for air masses originating from the Atlantic. However, no quantitative comparisons to measurements in the present study are possible due to the differences in measured particle size range. A similar influence of the air mass origin on measured inorganic mass concentrations was found for the AMS measurements performed during the MEGAPOLI winter campaign in Paris in January/February 2010 (Crippa et al., 2013a). Therefore, this strong dependency of inorganic mass concentrations on air mass origin seems to be a general feature valid throughout the year.

Generally no strong differences are observed between the three sampling stations for the more regionally homogeneously distributed secondary species. However, from the direct comparison of the time series, one event in SO_4 and several events in NO_3 time series can be observed where mass concentrations measured at the three stationary sites differ significantly (meaning beyond the uncertainty) from each other (Fig. 4). Such events either indicate that slightly different air masses were probed at the sites, or could be due to gas phase precursors of rather local origin, e.g. nearby SO_x emissions that do not affect all sampling locations in the same way. Such events are not reflected in the total averages, as those time periods are very short compared to the overall sampling time. Two significant events in the SO_4 time series can be identified to be due to the fireworks on 13 and 14 July. These events are visible at the Downtown and Sub NE site to a different extent, and not at all at the Sub SW site. During both time periods, wind direction was predominantly from the south (135–247.5°), such that the Sub NE site was much more affected by the surrounding fireworks than the other sites. Similarly large contributions of fireworks aerosol to SO_4 and organics mass concentrations have already been found by Drewnick et al. (2006).

Oxygenated organic aerosol (OOA): also for OOA, similar mass concentrations are found at all three stationary sites throughout the campaign, and different average mass concentrations are found for different types of air masses. However, in contrast to the inorganic species described above, here also different average mass concentrations are found between the two types of "Atlantic" air masses: OOA average mass concentration increases with increasing continental contribution, i.e. with lower wind speed and resulting prolonged residence time over the continent. This different behaviour of OOA compared to SO_4 is explainable both by other emission sources (both biogenic and anthropogenic) as well as other chemistry (faster conversion into oxidized and condensable species). This difference in behaviour is also reflected in the diurnal cycle of OOA observed at the stationary sites (Fig. 6). While SO_4 shows no strong diurnal cycle, a clear diurnal pattern is found for OOA for all sites and air masses. Starting around noon, OOA mass concentration increases until a maximum is reached in the afternoon at about 16:00–17:00. This is explainable by secondary organic aerosol formation after photo-oxidation of precursors (Ait-Helal et al., 2013), leading to condensation on the pre-existing particles, but potentially also to new particle formation. After photo-oxidation declines due to decreasing sunlight, the generation of newly formed OOA is reduced and existing OOA is diluted, causing a decline in the OOA diurnal cycle mass concentrations. During the night, both ambient temperature and the boundary layer height are decreasing, so more semi-volatile OOA is condensing onto existing particles and the particle number concentration is enhanced due to the shallower boundary layer. Rising boundary layer height and temperature in the morning lead to dilution of the particles and to re-evaporation of such semi-volatile species, similar to the temporal variation of NO_3 (see Fig. 7). However, in comparison with the advected, regionally distributed OOA (as discussed above), the possible contribution of such locally generated OOA is small. The predominantly regional character of OOA (as well

as of SO_4) has also been reported for the REPARTEE campaigns, which were conducted in autumn 2006 and 2007 in the London metropolitan area (Harrison et al., 2012). Here as well, only a small influence on measured OOA mass concentrations from local production has been found. This suggests that the findings from this study might not only be valid for Paris in summertime, but also to some extent for other large European urban agglomerations in different seasons.

As mentioned above, the diurnal cycle of OOA shows an increase in OOA mass concentration around noon, when also indications for particle growth are observed in the diurnal cycle of the EAS size distributions. Sources of these growing particles may either be freshly nucleated particles (with unknown composition), or small particles originating from primary emissions (e.g., engine exhaust). This larger abundance of smaller particles is consistent with simultaneously increasing number concentration measured by the CPC, reaching its maximum around 16:00–17:00 (Fig. 5b, all measured at Sub NE). These events must be taking place over extended areas, as the probed air masses are not stagnant, but constantly moving over the stationary measurement site at wind speeds of about 2.6 m s^{-1} (average value). Other features present in the EAS diurnal cycle are likely associated with coagulation and primary emissions: Starting at about 18:00–19:00 and lasting until about midnight, large number concentrations of particles with mobility diameters between about 40 and 200 nm are detected; the same is observed in the morning from about 06:00–11:00. Both peaks correspond to the peaks in the diurnal cycles of primary emission tracers. After midnight, the particle number concentration decreases, and also the particle size distribution changes, and particles smaller than about 50 nm decrease in number concentration. Air masses were not totally stagnant even during night time, but wind speeds were very low, such that this behaviour is more likely explained by coagulation than by dilution. The temporal behaviour agrees quantitatively with estimations for the loss rate of small particles by collision with the surface of larger particles following (Hinds, 1999) (Sect. S1 and Fig. S10 in the Supplement).

A comparison of size distributions from different instruments for different air masses is provided in the next section.

3.3.2 Size distribution characteristics

Size distributions were measured at all three stationary sites; however, to be able to compare distributions from different sites, thorough intercomparison experiments between the instruments are needed, which is outside the scope of this analysis. Here, we discuss only characteristics of size distributions for the different types of air masses. All size distributions presented here were measured at the Sub NE site.

For the three different types of air masses, median mass size distributions (meaning the median with respect to the time series of the size distribution) of species measured with the AMS at Sub NE are shown in Fig. 8. During all air masses, organics, NO_3, SO_4, and NH_4 are found in a single mode at around 300 nm ("Atlantic" air masses) to 400 nm ("Central Europe" air masses) vacuum-aerodynamic diameter (d_{va}). This shift of the accumulation mode to larger size in the "Central Europe" air masses is consistent with the dominance of more aged aerosol particles within these highly continentally influenced air masses. According to their size distributions, organics, NO_3, SO_4, and NH_4 seem to be internally mixed within the accumulation mode, which would be in line with the assumption of aged material. For the organics, a second, externally mixed smaller mode is observed. This mode could be caused by fresh primary emissions, e.g. of traffic exhaust, as has been found before (e.g., Zhang et al., 2005; Drewnick et al., 2004a). In Fig. 8, indicated with a grey line, the two organic modes have been divided at 259 nm d_{va}, the minimum between both modes, as a best estimate. Assuming spherical particles and a density of 1.59 g cm^{-3} as calculated from the average chemical composition measured with the AMS, this diameter corresponds to a mobility diameter of 163 nm (DeCarlo et al., 2004). This agrees with the particle size range of 40–200 nm for which in the diurnal cycle of the size distributions measured with the EAS distinct peaks were found, which were attributed to primary emissions (Fig. 5b, Sect. 3.3.1). Also shown in Fig. 8 are the contributions to the total organics mass concentration by particles smaller and larger than 259 nm d_{va}, i.e. by the fresh exhaust-related and the aged particles, respectively. This separation on the basis of the mass size distribution agrees well (within 6 %) with the contribution of the mass concentrations of HOA and OOA to the total organics mass concentration for the respective air masses determined using PMF analysis. These contributions, calculated from the median mass concentrations of HOA and OOA retrieved using PMF analysis, were 23.8 % HOA and 76.2 % OOA for "Central Europe"; 43.3 % HOA and 56.7 % OOA for "Atlantic Polluted"; and 50.6 % HOA and 49.4 % OOA for "Atlantic Clean". All these considerations seem to support the assumptions of primary emissions (represented by HOA) being dominant in the smaller organic mode (i.e., $d_{va} \leq 259$ nm), and of secondary organics (represented by OOA) being dominant in the larger size mode, internally mixed with inorganic, secondary species. Likely due to the fact that also species of the respective other type are mixed into each of the size fractions, mass spectra from the first and the second organic mode show no strong differences. Even m/z 44, which would indicate dominance of more aged organic aerosol particles (Aiken et al., 2008), is only insignificantly enhanced in the larger size mode. Also the size distributions of the mass spectral markers m/z 57 (traffic-related HOA) and m/z 44 (OOA) do not show a clear structure. This might be due to both the aforementioned potential slight mixture as well as to the influence

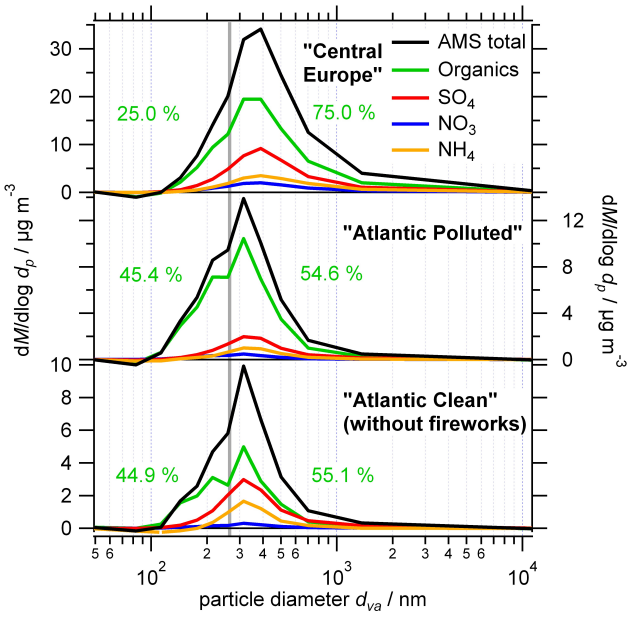

Fig. 8. AMS median mass size distributions for different air masses, measured at Sub NE. For the "Atlantic Clean" air masses size distributions, time periods influenced by fireworks were excluded. For organics size distributions, only m/z's up to m/z 100 were used to reduce noise. The "AMS total" is the sum of the species shown. Chloride showed no significant signal during any of the air masses. The AMS size distributions shown are scaled to the median of the measured mass concentrations for the respective time period and species. Given in the graph (green numbers) are the mass contributions to the total organics from particles in the size range $d_{va} \leq 259$ nm (left) and $d_{va} > 259$ nm (right). The size of 259 nm d_{va} is marked with a grey vertical line.

of cooking-related HOA, which shows less significant signal of m/z 57, but a larger influence of m/z 44 than traffic-related HOA (compare Fig. S5). To resolve HOA and OOA also in the size distributions, more sophisticated tools like three-dimensional PMF would be needed, as has recently been applied to AMS data by Ulbrich et al. (2012).

A comparison of particle size distributions for the different air masses measured with different instruments at Sub NE is given in Fig. 9. Particle volume size distributions (panels d–f) determined from the measurements of the different instruments agree within 10 %. Only the OPC distribution shows a larger discrepancy of about 20 % on average, likely due to the fact that the optical diameter measured by this instrument is not fully comparable to those of other instruments' measurements. In the particle number size distributions (panels a–c), all instruments agree above 200 nm d_{mob}. However, significant differences are observed between the AMS and the EAS below 200 nm d_{mob}. These differences could be due to additional uncertainty from the conversion of the measured AMS mass size distribution to a number size distribution, for which spherical particles with a size-dependent density (calculated from the respective chemical composition as measured with the AMS) were assumed. Other reasons could be a higher relative abundance of refractory species BC, which is not detected by the AMS, in the smaller particle size mode, or sampling losses, both in the AMS sampling lines and the instrument itself. This is likely the reason especially for the underestimation of the very small particles below $d_{va} = 70$ nm, because these are very inefficiently transmitted through the AMS inlet system to the AMS vaporizer (Liu et al., 2007). Uncertainties of the EAS number concentrations (see Sect. 2.2.1) additionally contribute to the differences.

When comparing the particle size distributions from all instruments for different air masses, the strongest differences in the particle volume size distributions are found in the measured total particle volume concentrations. The total particle volume concentration is highest for "Central Europe" and lowest for "Atlantic Clean" air masses, especially in the submicron size range. This agrees with the average aerosol mass concentrations measured with the AMS, as described in Sect. 3.3.1. Furthermore, AMS as well as EAS size distributions both show a shift of the maximum submicron particle volume concentration to larger diameters for the "Central Europe" air masses, as described above for the AMS only.

In the EAS number size distributions (Fig. 9a–c), differences between different air masses are more distinct. First of all, due to the reasons described above, the accumulation mode is shifted to larger particle sizes for the "Central Europe" air masses compared to the "Atlantic" air masses. Furthermore, differences in the absolute values of the number concentrations in the accumulation mode are observed between the two "Atlantic" air masses, while nucleation mode particles (between 10 and 20 nm d_{mob}) show similar number concentrations for all three air masses. However, as discussed in Sect. 2.2.1, the number concentrations measured by the EAS for the smallest particle sizes have to be regarded with higher uncertainty. In Fig. 10, medians of the EAS number size distributions measured at Sub NE during "Atlantic" air masses are presented, binned for different associated wind speeds. The normalized size distributions (Fig. 10, upper panel) show a clear wind speed dependence of the shape of the distributions. At low wind speed ($< 0.4\,\mathrm{m\,s^{-1}}$), the accumulation mode dominates the size distribution, while the nucleation mode is rather weak. With increasing wind speeds the relative intensity of the accumulation mode decreases and the nucleation mode dominates the size distribution more and more until at a wind speed of about $2\,\mathrm{m\,s^{-1}}$ the shape of the distribution remains stable. From this point on a further increase in wind speed only results in a reduction of the absolute number concentrations at all particle sizes (Fig. 10, lower panel).

These observations can be explained by a combination of dilution and residence time influences. At low wind speeds, due to the prolonged residence time of a given air mass over polluted areas, more particles and precursor gases are picked

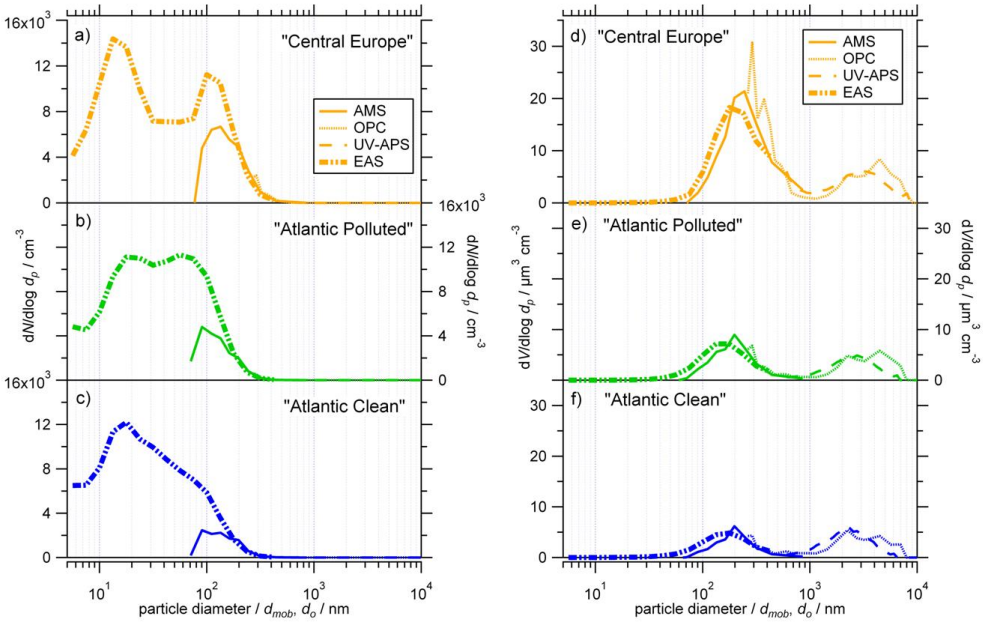

Fig. 9. Size distributions (median) for the different air masses, measured at Sub NE with AMS, EAS, OPC, and UV-APS. **(a–c)** dN/dlog d_p, **(d–f)** dV/dlog d_p. AMS total mass is converted to dV/dlog d_p, and AMS d_va to d_mob assuming a size-dependent density (derived from the chemical composition measured with the AMS). UV-APS d_ca is converted to d_mob assuming an average density of 1.65 g cm^{-3} (from the average chemical composition from AMS and BC measurements). dV/dlog d_p of EAS, OPC, and UV-APS is calculated from the measured dN/dlog d_p, and vice versa for the AMS.

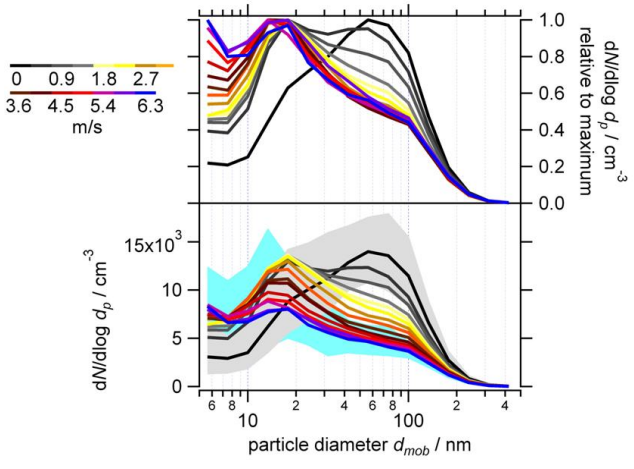

Fig. 10. EAS median number size distributions for different wind speeds. Upper panel: normalized to the highest value; lower panel: absolute values. Median size distributions of only the "Atlantic" air masses are shown; only wind speeds are included which were measured for at least 100 min. Percentiles (25 and 75 %) are shown exemplarily for wind speeds of 0 m s^{-1} (light grey) and 6.3 m s^{-1} (light blue).

up along its way towards the measurement site. In other words, under such low wind speed conditions emissions are less diluted. In addition, during calm periods sufficient time is provided for small particles to grow by coagulation and potentially condensation of secondary species before arrival at the site. This is further facilitated by the increased absolute levels of both particle number and surface concentrations as well as precursor gas concentrations under such conditions due to reduced dilution. From theory (following Hinds, 1999), it can be estimated that coagulation of the smaller particles would take about one hour to reach the size distribution observed during calm periods (Sect. S1 and Fig. S11 in the Supplement).

Both factors are consistent with the observations of median number size distributions for the two "Atlantic" air masses (Fig. 9b and c): during "Atlantic Clean" air masses, a high average wind speed is found, together with a diminished accumulation mode compared to the size distribution observed for the "Atlantic Polluted" air masses, which also arrive from a western wind direction at the measurement site, but are characterized by a lower average wind speed.

No wind speed dependency is found for the supermicron particle concentrations, although at higher wind speeds, resuspension of coarse mode particles would be expected. Likely, higher wind speeds than typically encountered throughout the measurement campaign would be needed for an efficient resuspension of supermicron particles.

3.4 Background measurement: a case study

On 15 July 2009 ("Atlantic Clean" air masses), a stationary measurement of the Mobile Laboratory was taking place

Table 4. Average mass concentrations and volume mixing ratios along with associated uncertainties for the time period of the Mobile Laboratory (MoLa) background measurement (15 July, 14:30 to 20:32).

Species		MoLa	Sub SW	Downtown	Sub NE
BC	($\mu g\ m^{-3}$)	0.10 ± 0.01	0.41 ± 0.12	0.78 ± 0.08	0.59 ± 0.06
NO_x	(ppb)	0.3 ± 0.1	5.6 ± 1.1	10.4 ± 2.1	7.3 ± 1.5
HOA	($\mu g\ m^{-3}$)	0.34 ± 0.12	0.31 ± 0.11	1.27 ± 0.46	0.86 ± 0.31
OOA	($\mu g\ m^{-3}$)	0.96 ± 0.35	0.80 ± 0.29	0.98 ± 0.35	0.97 ± 0.35
SO_4	($\mu g\ m^{-3}$)	1.54 ± 0.41	1.12 ± 0.34	1.29 ± 0.39	1.00 ± 0.30
NO_3	($\mu g\ m^{-3}$)	0.14 ± 0.04	0.12 ± 0.04	0.17 ± 0.05	0.09 ± 0.03
O_3	(ppb)	42.7 ± 4.3	41.5 ± 4.2	40.1 ± 4.0	42.7 ± 4.3

from 14:30 to 20:30 local time at the location denoted in Fig. 1 (1°47′46.21″ E, 48°23′24.34″ N). This measurement location was upwind from the Paris metropolitan area throughout the whole measurement time (wind direction measured at the Mobile Laboratory: 194–264°) and located sufficiently far away from the city and any nearby sources to qualify as a real background site without any urban influence. This enables the differentiation between pollutants dominated by emissions within the urban agglomeration and pollutants which are transported from outside the city to Paris.

Averages of different tracer concentrations measured at all stationary sites and the Mobile Laboratory during this time frame are presented in Table 4 and Fig. 11. Within the uncertainties, averages of SO_4, NO_3, and OOA mass concentrations, and of O_3 volume mixing ratios are the same at all four measurement locations. This validates further the assumption from Sect. 3.3.1 that these species are regionally homogeneously distributed over the greater Paris region and not significantly influenced by emissions from the Paris agglomeration. On the other hand, while smaller mass concentrations of HOA and BC, and volume mixing ratios of NO_x are measured at Sub NE and Sub SW than at the Downtown site, concentrations measured at the background station are even much smaller than measured at the suburban sites. This reflects the fact that also the suburban measurement sites are heavily influenced by local emissions, as was already concluded in Sect. 3.3.1. Therefore, as both suburban sites are influenced by local emissions, it is not straightforward to decide whether differences in concentrations measured at Sub NE and Sub SW are due to pollution advected from the whole Paris agglomeration, or originate from slight differences in local emissions. This issue is addressed further in the following section.

3.5 Examination of the Paris emission plume

To reliably examine the influence of the emission plume of Paris on the suburban stationary sites, quasi-Lagrangian measurements under connected flow conditions are required. Wind directions of $45 \pm 11.25°$ (NE) represent a connected flow from Sub NE over Downtown to Sub SW, while wind

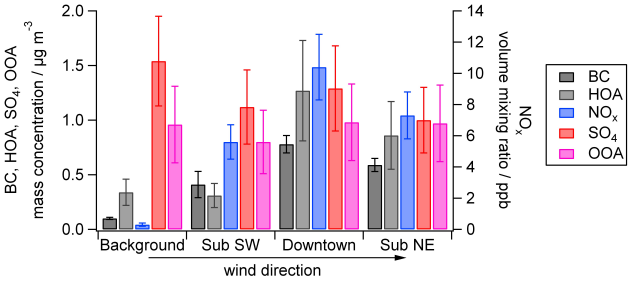

Fig. 11. Average mass concentrations (BC, HOA, SO_4, OOA) and volume mixing ratios (NO_x) measured at the three stationary sites and at a background location (see Fig. 1) during the background measurement case study (15 July, 14:30 to 20:32; "Atlantic Clean" air masses). Error bars represent the associated estimated uncertainties for intercomparison purposes (see Sect. 2). The arrow indicates the wind direction of the connected flow during the measurement period. The exact values and additional data from NO_3 and O_3 are given in Table 4.

directions of $225 \pm 11.25°$ (SW) represent a connected flow from Sub SW over Downtown to Sub NE. To exclude influences of air mass origin and meteorology (as discussed in Sect. 3.3) as far as possible, only measurements during the same type of air mass were compared. This was possible since occasionally, for short time periods the local wind direction measured in the Paris region was different from the overall, dominant wind direction associated with the air mass origin. During times when the "Central Europe" air masses were sampled, Sub SW was predominantly located downwind of Paris, while during times when "Atlantic Clean" air masses were sampled, Sub NE was predominantly located downwind. Therefore, "Atlantic Polluted" air masses were chosen for this analysis, in order to have sufficient measurement time for both Sub NE (1248 min) and Sub SW (797 min) being downwind of Paris while all instruments were operating.

Averages for measured species concentrations from all sites for the two cases Sub NE/Sub SW being downwind of the city centre are presented in Table 5 and Fig. 12. In both cases, the secondary species SO_4, NO_3, OOA, and O_3 show

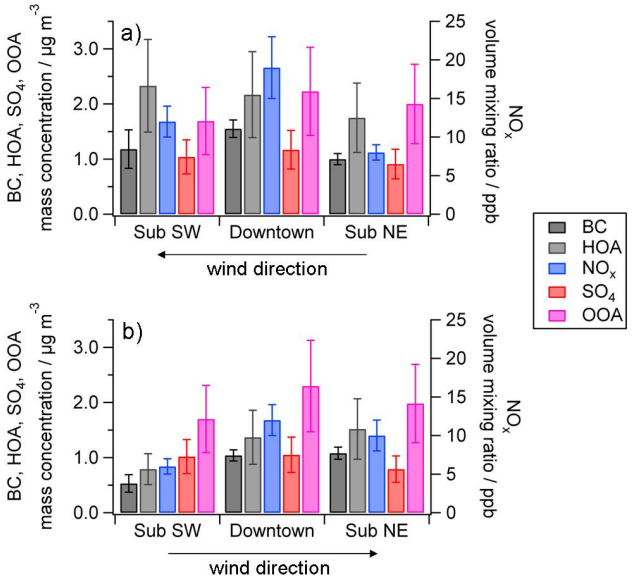

Fig. 12. Average mass concentrations (BC, HOA, SO_4, OOA) and volume mixing ratios (NO_x) measured at the three stationary sites during "Atlantic Polluted" air masses for quasi-Lagrangian measurements at connected flow conditions with **(a)** Sub SW downwind, **(b)** Sub NE downwind of the city centre. Error bars represent the associated estimated uncertainties for intercomparison purposes (see Sect. 2). The arrows indicate the wind direction of the connected flow during the measurement periods. The exact values and additional data from NO_3 and O_3 are given in Table 5.

Table 5. Averages of selected species measured at the stationary sites from quasi-Lagrangian measurements at connected flow conditions during "Atlantic Polluted" air masses with Sub SW and Sub NE being downwind of the city centre, respectively.

Sub SW downwind				
Species		Sub SW	Downtown	Sub NE
BC	($\mu g\,m^{-3}$)	1.18 ± 0.35	1.55 ± 0.16	1.00 ± 0.10
NO_x	(ppb)	12 ± 2	19 ± 4	8 ± 1
HOA	($\mu g\,m^{-3}$)	2.33 ± 0.84	2.17 ± 0.78	1.75 ± 0.63
OOA	($\mu g\,m^{-3}$)	1.69 ± 0.61	2.23 ± 0.80	2.00 ± 0.72
SO_4	($\mu g\,m^{-3}$)	1.04 ± 0.31	1.17 ± 0.35	0.91 ± 0.27
NO_3	($\mu g\,m^{-3}$)	0.25 ± 0.08	0.33 ± 0.10	0.21 ± 0.06
O_3	(ppb)	23 ± 2	25 ± 3	26 ± 3
Sub NE downwind				
Species		Sub SW	Downtown	Sub NE
BC	($\mu g\,m^{-3}$)	0.53 ± 0.16	1.04 ± 0.10	1.08 ± 0.11
NO_x	(ppb)	6 ± 1	12 ± 2	10 ± 2
HOA	($\mu g\,m^{-3}$)	0.79 ± 0.28	1.37 ± 0.49	1.52 ± 0.55
OOA	($\mu g\,m^{-3}$)	1.70 ± 0.61	2.30 ± 0.83	1.98 ± 0.71
SO_4	($\mu g\,m^{-3}$)	1.02 ± 0.31	1.05 ± 0.32	0.79 ± 0.24
NO_3	($\mu g\,m^{-3}$)	0.16 ± 0.05	0.24 ± 0.07	0.20 ± 0.06
O_3	(ppb)	36 ± 4	34 ± 3	37 ± 4

the same mass concentrations and volume mixing ratios, respectively, within their uncertainties at all sites. Again, this shows the regional distribution of these species. On the other hand, the primary emission tracers BC and NO_x show different average mass concentrations and volume mixing ratios, respectively, at the different sites. For HOA, although a primary emission tracer, the associated uncertainties are too high to allow the detection of any significant differences. In the case of Sub NE being downwind of the city centre, similar average concentrations of primary emission tracers at both the Sub NE and the Downtown site are observed, while lower average concentrations are observed at the Sub SW site. In the case of Sub SW being downwind, the BC mass concentration of Sub SW is within the uncertainty comparable to both other sites, while the BC mass concentration measured at Sub NE is much smaller than measured at the Downtown site. The NO_x volume mixing ratio is highest at the Downtown site, and lowest at Sub NE, with Sub SW volume mixing ratio being almost comparable to the one measured at the Downtown site. This behaviour of measured mass concentrations and volume mixing ratios for the different wind directions indicates that indeed when the suburban sites are downwind of the Paris city centre, they are more strongly influenced by advected emissions from the city and greater Paris region. This primary emission tracer plume, however, is observed on top of the already large concentrations of associated tracers from local emissions in the environment of the suburban sites. Therefore, only very rough estimates can be given for the relative contribution of advected pollution to the downwind sites. As an upper limit for the plume impact onto the suburban sites, the measurements at the respective downwind sites can be used as an estimate. These are approximately volume mixing ratios of 8–14 ppb of NO_x, and mass concentrations of about 1–1.5 $\mu g\,m^{-3}$ of BC and of about 1–3 $\mu g\,m^{-3}$ of HOA, containing both locally produced emissions and emissions advected from the Paris agglomeration to the suburban site. As a lower limit, the difference between concentrations measured at the respective downwind and upwind site can be used, assuming as a best estimate that local emissions at the upwind site are comparable to the ones at the downwind site. This results in lower limits of 0–1 $\mu g\,m^{-3}$ of BC, 0–2 $\mu g\,m^{-3}$ of HOA, and 1–7 ppb of NO_x. Therefore, for the emission plume impact on the suburban sites, all in all a rough estimate of 1–14 ppb of NO_x, and upper limits of 3 $\mu g\,m^{-3}$ of HOA, and of 1.5 $\mu g\,m^{-3}$ of BC can be given from this analysis. The broad range of these estimates does not only reflect the uncertainty from the used approach, but also the high temporal variability of local emissions. Still, these estimates represent only very rough approximations of the order of magnitude as they are heavily influenced by local emissions. To be able to really quantify the impact of the Paris emission plume on the affected downwind area, not only longer time periods of connected flow conditions

Table 6. Selected results from measurements in megacities worldwide. Values represent the averages over the respective measurement period; values in parentheses represent the lowest and highest value observed.

City, country	Measurement period	NH_4/ µg m^{-3}	SO_4/ µg m^{-3}	NO_3/ µg m^{-3}	Organics/ µg m^{-3}	BC (or EC[a])/ µg m^{-3}	NO_x/ ppb	O_3/ ppb
London, England	Oct 2006[b]	(∼ 0–7)	(∼ 0–11.5)	(∼ 0–13)	(∼ 0–19)	(∼ 0–10)	29–109 (∼ 0–420)	4–14 (∼ 0–50)
	Oct/Nov 2007[b]	(∼ 0–11)	(∼ 0–10)	(∼ 0–27)	(∼ 0–54)	(∼ 0–15)	26–166 (∼ 0–600)	4–32 (∼ 0–60)
Paris, France	Jan/Feb 2010[c,d]	2 (∼ 0–10)	2–3 (∼ 0–20)	4–5 (∼ 0–27)	5–6 (∼ 0–30)	1–2 (∼ 0–16)	(∼ 0–200)	n/a
	Jul 2009 (this study)[c]	0.4–0.6 (< D.L.[e]–5.7)	1.3–1.4 (< D.L.–17.3)	0.3–0.4 (< D.L.–13.7)	2.6–3.9 (0.05–442.4)	0.7–1.4 (< D.L.–16.2)	7–17 (< D.L.–185)	29–30 (< D.L.–108)
New York City, USA	Jan/Feb 2004[f]	1.65 (< D.L.–9.11)	2.41 (0.34–9.74)	2.58 (0.06–19.61)	4.80 (< D.L.–33.75)	n/a	(∼ 10–210)	n/a
	Jul/Aug 2001[f]	1.70 (< D.L.–12.46)	3.85 (0.01–54.26)	0.68 (< D.L.–9.55)	5.98 (< D.L.–64.95)	n/a	n/a	n/a
	Jul/Aug 2009[g]	1.28 (0.06–3.67)	2.82 (0.13–12.1)	0.49 (0.03–4.44)	6.34 (1.03–27.7)	0.70 (< D.L.–6.21)	(∼ 0–180)	n/a
Los Angeles Basin, USA	Jun–Aug 2009[h]	(∼ 0–7)	(∼ 0–14)	(∼ 0–15)	(∼ 1– 20)	n/a	(∼ 10–120)	(∼ 0–120)
Tokyo, Japan	Jan/Feb 2004[i]	2.7 (∼ 0–7)	1.8 (∼ 0–4)	3.9 (∼ 0–11)	∼ 7 (∼ 0–17)	n/a	38.4 (22.2–58.0)	15.4 (3.8–28.4)
	Jul/Aug 2003[i]	1.9 (∼ 0–5)	3.2 (∼ 0–8)	1.5 (∼ 0–10)	∼ 7 (∼ 1–17)	n/a	14 (9.5–20.6)	16.5 (5.8–29.6)
Mexico City, Mexico	Apr 2003[j]	2.2 (< D.L.–14.8)	3.1 (< D.L.–22.7)	3.7 (0.1–49.0)	21.6 (1.3–106.5)	3.4 (0.2–52.7)	31	n/a
	Mar 2006[k]	2.0 (∼ 0–10)	3.6 (∼ 0–17)	3.5 (∼ 0–26)	17.3 (∼ 0–82)	4.2 (∼ 0–24)	n/a	n/a
Beijing, China	Jul 2006[l]	13.1 (0.27–42.7)	20.3 (0.23–82.3)	17.3 (0.5–79.2)	28.1 (1.2–99.9)	n/a	n/a	n/a

[a] EC: elemental carbon.
[b] REPARTEE campaigns, (Allan et al., 2010; Harrison et al., 2012). For NO_x and O_3, ranges of averages and of lowest and highest values measured at different measurement sites are given.
[c] Given as "average" is the range of averages measured at the three measurement sites; lowest and highest values represent the range of lowest to highest values observed at all three sites.
[d] MEGAPOLI winter campaign, (Crippa et al., 2013a).
[e] Detection limit.
[f] PMTACS-NY, (Drewnick et al., 2004b; Weimer et al., 2006).
[g] (Sun et al., 2011).
[h] PACO, (Hersey et al., 2011).
[i] (Takegawa et al., 2006b; Jimenez et al., 2009). For NO_x and O_3, instead of averages, median values and percentiles (25 and 75 %) are given.
[j] MCMA-2003, (Salcedo et al., 2006; Dunlea et al., 2007).
[k] MILAGRO, (Aiken et al., 2009).
[l] (Sun et al., 2010).

for quasi-Lagrangian measurements would be needed to get statistically more significant estimates, but also plume measurements in more remote locations without impact of local emissions. Such measurements are available for this campaign from the Mobile Laboratory measurements, and are presented in (von der Weiden-Reinmüller et al., 2013).

3.6 Comparison to other megacities

In Table 6, a compilation of results from measurement campaigns in megacities worldwide is shown. Compared are mass concentrations of NH_4, NO_3, SO_4, and organics as measured with the AMS, BC, and volume mixing ratios of NO_x and O_3. Results from summer and winter campaigns are shown. As a general feature, total mass concentrations (of AMS and, if available, BC, the sum of both nearly corresponding to PM_1) were comparable (in the range of less than 10 up to about 20 µg m^{-3}) between the European megacities London and Paris, the North American megacities New York and the Los Angeles Basin, and the Asian megacity Tokyo. With about 30 µg m^{-3} during the selected measurement campaigns, total PM_1 mass concentrations were somewhat higher in Mexico City (Central America), while the by far highest average PM_1 mass concentrations with about 80 µg m^{-3} were observed in Beijing in Asia. However, it has to be kept in mind that the chosen measurement locations might be very different. Locations in the centre of the city with a strong traffic impact are susceptible to higher concentrations of primary emission tracers than measurement locations e.g. in the suburbs or further away from major traffic lines. This is obvious in the range of volume mixing ratios given for NO_x for the London campaigns, where a range of values measured at different sites (located e.g. close to a major road and in a park) is given: values from about 20 up to about 150 ppb are observed on average at such different locations. Furthermore, season has a strong effect on measured mass concentrations. This is obvious for the NO_3 mass concentrations, which generally are higher for the winter campaigns when compared to the summer campaigns in the same city (e.g., less than 0.5 µg m^{-3} in Paris in this study, and 4–5 µg m^{-3} for the winter campaign, Crippa et al., 2013a). For organics, it can be expected that secondary organic aerosol formation is more effective in summer than in winter, favouring higher particulate organic mass concentrations. However, also primary emissions are composed of organics, and while not only more primary emissions due to e.g. domestic heating are expected for wintertime, also the boundary layer conditions in wintertime favour accumulation of primary emissions, leading to higher observed mass concentrations of organics. Likely for these two counter-acting influences of season on particulate organics mass concentrations, all in all, organics mass concentrations were rather comparable for the different seasons within a certain city. Furthermore, it has to be noted that the compared measurement periods were rather

short (usually in the order of about one month), and measured average mass concentrations are not necessarily representative for the respective locations and seasons.

In Mexico City, where somewhat higher total mass concentrations were observed, a slightly larger fraction of the total mass was due to organics (about 60 % as opposed to typically 40–50 % in the aforementioned cities). This could both be due to stronger secondary organic aerosol formation as a consequence of larger precursor emissions and increased photochemical activity, and to larger primary emissions of particulate organic material. Mass concentrations of inorganic material, on the other hand, were rather comparable to values typically observed during wintertime campaigns in the aforementioned cities. In contrast, in Beijing, where by far the highest average mass concentrations were observed, the organic fraction was comparable to European and other megacities; NO_3, however, was making up a large fraction of the total mass even during this summertime campaign. This is explainable by less emission control of inorganic species in China compared e.g. to Europe or North America (Hill, 2010). This indicates that while in Beijing emission control of inorganic species still can have a strong influence on the average PM_1 mass concentration, this is true to a lesser extent for Central and North America and Europe, where these emissions are already largely regulated (Hill, 2010). Here, the organic mass fraction plays a much larger role for the total aerosol burden. This is in line with the observations of this study, which indicated a large regional control of PM_1 species even within the megacity of Paris, and only a comparably small fraction of PM_1 originating from primary emissions within the city.

4 Summary and conclusions

A one-month measurement campaign was performed during July 2009 in and around the megacity of Paris. Three stationary sites were operated, enabling the measurement of spatial differences of selected pollutants. Air mass origin was found to have the main influence on measured OOA, SO_4, NO_3, and NH_4 mass concentrations and O_3 volume mixing ratio. These typical secondary species were regionally distributed over the greater Paris region, and did not seem to be significantly influenced by local emissions at the individual sites. On the other hand, apart from diurnal source strength variations and proximity to emission sources, local meteorology was found to be the main factor influencing the measured mass concentrations of BC and HOA, and the volume mixing ratio of NO_x. At higher wind speeds, dilution processes led to lower concentrations of these primary emission tracers, which were found to be originating predominantly from the city itself. Differences in wind speed also had influence on the measured submicron particle number size distribution, with an increased wind speed diminishing especially the number of accumulation mode particles.

It was found that the secondary species OOA, SO_4, NO_3, and NH_4 as well as O_3 were regionally distributed over the greater region with no significant differences observed between the three sampling stations. This finding was supported by a case study that included also background measurements farther upwind of the agglomeration using a mobile laboratory. The OOA mass concentration observed at the sites was largely influenced by the residence time of the sampled air mass over the continent. Furthermore, diurnal cycles of OOA mass concentrations and of particle number size distributions indicated a small local contribution of secondary organic aerosol formation (leading to condensation and particle growth) to the OOA mass concentration and possibly a small fraction of semi-volatile OOA partitioning between gas and particle phase. This local effect, however, was either too small to be visible in averages over longer time periods, or else it was present at all stationary sites to a similar extent. The dominating fraction of OOA, however, seemed to be of regional rather than local origin, similar to the findings from the REPARTEE campaigns in London (Harrison et al., 2012). The average mass concentrations of secondary species were elevated during time periods with air masses being advected from Central Europe, in agreement with other studies (Crippa et al., 2013a; Sciare et al., 2010) as described in Sect. 3.3.1. This all together indicates that the findings presented in this paper are likely not only valid for Paris in summertime, but also to some extent for other seasons and for other large European urban agglomerations. Further measurements in other European urban agglomerations would be desirable to further generalize this finding.

From quasi-Lagrangian measurements at the three stationary sites during connected flow conditions, a small influence by the Paris emission plume on local air composition was detectable. However, due to local emissions at the suburban downwind and upwind sites themselves, only very rough estimates for contributions of primary emission tracers NO_x, BC, and HOA advected from the Paris region can be deduced. Volume mixing ratios of 1–14 ppb of NO_x, and upper limits for mass concentrations of about $1.5\,\mu g\,m^{-3}$ of BC and of about $3\,\mu g\,m^{-3}$ of HOA were determined, originating both from local emissions and from the overall Paris emission plume. Further work is needed to quantify the Paris emission plume downwind of the city without influence of local emissions.

Appendix A

List of abbreviations

AMS	Aerodyne aerosol mass spectrometer
APS	Aerodynamic particle sizer
BC	Black carbon
CE	Collection efficiency
Chl	Particulate chloride as measured by the AMS
CPC	Condensation particle counter
C-ToF-AMS	Compact time-of-flight aerosol mass spectrometer
d_{ca}	Continuum-aerodynamic diameter
d_{mob}	Mobility diameter
d_o	Optical diameter
d_{va}	Vacuum-aerodynamic diameter
EAS	Electrical aerosol spectrometer
FMPS	Fast mobility particle sizer
HOA	Hydrocarbon-like organic aerosol
$HOA_{cooking\_rel.}$	Cooking-related hydrocarbon-like organic aerosol
$HOA_{traffic\_rel.}$	Traffic-related hydrocarbon-like organic aerosol
HR-ToF-AMS	High-resolution time-of-flight aerosol mass spectrometer
IC	Ion chromatography
IE	Ionisation efficiency
LIDAR	Light detection and ranging
MAAP	Multi-angle absorption photometer
MEGAPOLI	Megacities: Emissions, urban, regional, and Global Atmospheric POLlution and climate effects, and Integrated tools for assessment and mitigation
MoLa	Mobile Laboratory
MS	Mass spectra
NH_4	Particulate ammonium as measured by the AMS
NO_3	Particulate nitrate as measured by the AMS
OOA	Oxygenated organic aerosol
OPC	Optical particle counter
PILS-IC	Particle-into-liquid sampler coupled to an ion chromatograph
PMF	Positive matrix factorization
PToF	Particle time-of-flight
REPARTEE	Regents Park and Tower Environmental Experiment
RH	Relative humidity
RIE	Relative ionisation efficiency
SMPS	Scanning mobility particle sizer
SO_4	Particulate sulphate as measured by the AMS
Sub NE	Suburban north-east site
Sub SW	Suburban south-west site
TEOM-FDMS	Tapered element oscillating microbalance – filter dynamics measurement system
UV-APS	Ultraviolet aerodynamic particle sizer

Supplementary material related to this article is available online at: http://www.atmos-chem-phys.net/13/933/2013/acp-13-933-2013-supplement.pdf.

Acknowledgements. The authors thank T. Böttger, S. Gallavardin, P. Reitz, and J. Y. Schmale for support before and during the campaign. Thanks to U. Pöschl for providing a MAAP and an UV-APS, to S. Weinbruch for providing the EAS, and to R. Zimmermann for providing a HR-ToF-AMS. We are grateful to A. Huffman and K. Kandler for support regarding the data handling of the UV-APS and the EAS, respectively. The staff of the Golf de la Poudrerie is thankfully acknowledged, especially C. Pouette and E. Leroux for technical and logistical support throughout the campaign. We extend our acknowledgements to the technical and computer staff of the SIRTA observatory for taking the meteorological observations and making the dataset easily accessible. E. Kostenidou, L. Hildebrandt and B. H. Lee are gratefully acknowledged for providing the SMPS data at SIRTA. The LISA group is thankful to C. Afif, W. Ait-Helal, R. Durand-Jolibois, K. Miet, S. Perrier, C. Puente-Lelievre, and G. Siour for their contribution to the field campaign at the SIRTA site. We thank as well the staff of LHVP for hosting measurements and for technical and logistical support. ECMWF and met.no granted access to ECMWF wind fields. Parts of the presented research have received funding from the European Union's Seventh Framework Programme FP/2007-2011 within the project MEGAPOLI, grant agreement no. 212520, and from the French ANR MEGAPOLI-PARIS project. The participation of MPIC scientists in the campaign was fully covered by internal funds of MPIC.

The service charges for this open access publication have been covered by the Max Planck Society.

Edited by: J.-L. Jimenez

References

Aiken, A. C., DeCarlo, P. F., Kroll, J. H., Worsnop, D. R., Huffman, J. A., Docherty, K. S., Ulbrich, I. M., Mohr, C., Kimmel, J. R., Sueper, D., Sun, Y., Zhang, Q., Trimborn, A., Northway, M., Ziemann, P. J., Canagaratna, M. R., Onasch, T. B., Alfarra, M. R., Prevot, A. S. H., Dommen, J., Duplissy, J., Metzger, A., Baltensperger, U., and Jimenez, J. L.: O/C and OM/OC Ratios of Primary, Secondary, and Ambient Organic Aerosols with High-Resolution Time-of-Flight Aerosol Mass Spectrometry, Environ. Sci. Technol., 42, 4478–4485, doi:10.1021/es703009q, 2008.

Aiken, A. C., Salcedo, D., Cubison, M. J., Huffman, J. A., DeCarlo, P. F., Ulbrich, I. M., Docherty, K. S., Sueper, D., Kimmel, J. R., Worsnop, D. R., Trimborn, A., Northway, M., Stone, E. A., Schauer, J. J., Volkamer, R. M., Fortner, E., de Foy, B., Wang, J., Laskin, A., Shutthanandan, V., Zheng, J., Zhang, R., Gaffney, J., Marley, N. A., Paredes-Miranda, G., Arnott, W. P., Molina, L. T., Sosa, G., and Jimenez, J. L.: Mexico City aerosol analysis during MILAGRO using high resolution aerosol mass spectrometry at the urban supersite (T0) – Part 1: Fine particle composi-

tion and organic source apportionment, Atmos. Chem. Phys., 9, 6633–6653, doi:10.5194/acp-9-6633-2009, 2009.

Ait-Helal, W., Borbon, A., Sauvage, S., De Gouw, J. A., Colomb, A., Beekmann, M., Afif, C., Durand-Jolibois, R., Fronval, I., Grand, N., Leonardis, T., Michoud, V., Miet, K., Perrier, S., Siour, G., Zapft, P., Doussin, J.-F., Lopez, M., Gros, V., Freutel, F., Schneider, J., Crippa, M., Prévôt, A. S. H., Baltensperger, U., and Locoge, N.: I/VOC in sub-urban Paris: variability, origin and importance in SOA formation, to be submitted to Atmos. Chem. Phys. Discuss., 2013.

Allan, J. D., Delia, A. E., Coe, H., Bower, K. N., Alfarra, M. R., Jimenez, J. L., Middlebrook, A. M., Drewnick, F., Onasch, T. B., Canagaratna, M. R., Jayne, J. T., and Worsnop, D. R.: A generalised method for the extraction of chemically resolved mass spectra from Aerodyne aerosol mass spectrometer data, J. Aerosol. Sci., 35, 909–922, doi:10.1016/j.jaerosci.2004.02.007, 2004.

Allan, J. D., Williams, P. I., Morgan, W. T., Martin, C. L., Flynn, M. J., Lee, J., Nemitz, E., Phillips, G. J., Gallagher, M. W., and Coe, H.: Contributions from transport, solid fuel burning and cooking to primary organic aerosols in two UK cities, Atmos. Chem. Phys., 10, 647–668, doi:10.5194/acp-10-647-2010, 2010.

Butler, T. M., Lawrence, M. G., Gurjar, B. R., van Aardenne, J., Schultz, M., and Lelieveld, J.: The representation of emissions from megacities in global emission inventories, Atmos. Environ., 42, 703–719, 2008.

Canagaratna, M. R., Jayne, J. T., Jimenez, J. L., Allan, J. D., Alfarra, M. R., Zhang, Q., Onasch, T. B., Drewnick, F., Coe, H., Middlebrook, A., Delia, A., Williams, L. R., Trimborn, A. M., Northway, M. J., DeCarlo, P. F., Kolb, C. E., Davidovits, P., and Worsnop, D. R.: Chemical and microphysical characterization of ambient aerosols with the Aerodyne aerosol mass spectrometer, Mass Spectrom. Rev., 26, 185–222, 2007.

CONAGUA, Comisión Nacional del Agua, http://worldweather.wmo.int/179/c00279.htm, last access: November 2011.

Crippa, M., DeCarlo, P. F., Slowik, J. G., Mohr, C., Heringa, M. F., Chirico, R., Poulain, L., Freutel, F., Sciare, J., Cozic, J., Di Marco, C. F., Elsasser, M., Nicolas, J. B., Marchand, N., Abidi, E., Wiedensohler, A., Drewnick, F., Schneider, J., Borrmann, S., Nemitz, E., Zimmermann, R., Jaffrezo, J. L., Prévôt, A. S. H., and Baltensperger, U.: Wintertime aerosol chemical composition and source apportionment of the organic fraction in the metropolitan area of Paris, Atmos. Chem. Phys., 13, 961–981, doi:10.5194/acp-13-961-2013, 2013a.

Crippa, M., El Haddad, I., Slowik, J. G., DeCarlo, P. F., Mohr, C., Heringa, M. F., Chirico, R., Marchand, N., Sciare, J., Baltensperger, U., and Prévôt, A. S. H.: Identification of marine and continental aerosol sources in Paris using high resolution aerosol mass spectrometry, J. Geophys. Res., doi:10.1029/jgrd.50151, accepted, 2013b.

Cross, E. S., Slowik, J. G., Davidovits, P., Allan, J. D., Worsnop, D. R., Jayne, J. T., Lewis, D. K., Canagaratna, M., and Onasch, T. B.: Laboratory and Ambient Particle Density Determinations using Light Scattering in Conjunction with Aerosol Mass Spectrometry, Aerosol Sci. Technol., 41, 343–359, doi:10.1080/02786820701199736, 2007.

Dall'Osto, M., Ceburnis, D., Martucci, G., Bialek, J., Dupuy, R., Jennings, S. G., Berresheim, H., Wenger, J., Healy, R., Facchini, M. C., Rinaldi, M., Giulianelli, L., Finessi, E., Worsnop, D., Ehn, M., Mikkilä, J., Kulmala, M., and O'Dowd, C. D.: Aerosol properties associated with air masses arriving into the North East Atlantic during the 2008 Mace Head EUCAARI intensive observing period: an overview, Atmos. Chem. Phys., 10, 8413–8435, doi:10.5194/acp-10-8413-2010, 2010a.

Dall'Osto, M., Ceburnis, D., Martucci, G., Bialek, J., Dupuy, R., Jennings, S. G., Berresheim, H., Wenger, J. C., Healy, R. M., Facchini, M. C., Rinaldi, M., Giulianelli, L., Finessi, E., Worsnop, D., Ehn, M., Mikkilä, J., Kulmala, M., Sodeau, J., and O'Dowd, C. D.: Corrigendum to "Aerosol properties associated with air masses arriving into the North East Atlantic during the 2008 Mace Head EUCAARI intensive observing period: an overview" published in Atmos. Chem. Phys., 10, 8413–8435, 2010, Atmos. Chem. Phys., 10, 8549–8549, doi:10.5194/acp-10-8549-2010, 2010b.

DeCarlo, P. F., Slowik, J. G., Worsnop, D. R., Davidovits, P., and Jimenez, J. L.: Particle Morphology and Density Characterization by Combined Mobility and Aerodynamic Diameter Measurements. Part 1: Theory, Aerosol Sci. Technol., 38, 1185–1205, doi:10.1080/027868290903907, 2004.

DeCarlo, P. F., Kimmel, J. R., Trimborn, A., Northway, M. J., Jayne, J. T., Aiken, A. C., Gonin, M., Fuhrer, K., Horvath, T., Docherty, K. S., Worsnop, D. R., and Jimenez, J. L.: Field-Deployable, High-Resolution, Time-of-Flight Aerosol Mass Spectrometer, Anal. Chem., 78, 8281–8289, doi:10.1021/ac061249n, 2006.

Diesch, J.-M., Drewnick, F., Zorn, S. R., von der Weiden-Reinmüller, S.-L., Martinez, M., and Borrmann, S.: Variability of aerosol, gaseous pollutants and meteorological characteristics associated with changes in air mass origin at the SW Atlantic coast of Iberia, Atmos. Chem. Phys., 12, 3761–3782, doi:10.5194/acp-12-3761-2012, 2012.

Drewnick, F., Jayne, J. T., Canagaratna, M., Worsnop, D. R., and Demerjian, K. L.: Measurement of Ambient Aerosol Composition During the PMTACS-NY 2001 Using an Aerosol Mass Spectrometer. Part II: Chemically Speciated Mass Distributions, Aerosol Sci. Technol., 38, 104–117, doi:10.1080/02786820390229534, 2004a.

Drewnick, F., Schwab, J. J., Jayne, J. T., Canagaratna, M., Worsnop, D. R., and Demerjian, K. L.: Measurement of Ambient Aerosol Composition During the PMTACS-NY 2001 Using an Aerosol Mass Spectrometer. Part I: Mass Concentrations, Aerosol Sci. Technol., 38, 92–103, doi:10.1080/02786820390229507, 2004b.

Drewnick, F., Hings, S. S., DeCarlo, P., Jayne, J. T., Gonin, M., Fuhrer, K., Weimer, S., Jimenez, J. L., Demerjian, K. L., Borrmann, S., and Worsnop, D. R.: A New Time-of-Flight Aerosol Mass Spectrometer (TOF-AMS) – Instrument Description and First Field Deployment, Aerosol Sci. Technol., 39, 637–658, doi:10.1080/02786820500182040, 2005.

Drewnick, F., Hings, S. S., Curtius, J., Eerdekens, G., and Williams, J.: Measurement of fine particulate and gas-phase species during the New Year's fireworks 2005 in Mainz, Germany, Atmos. Environ., 40, 4316–4327, 2006.

Drewnick, F., Böttger, T., von der Weiden-Reinmüller, S.-L., Zorn, S. R., Klimach, T., Schneider, J., and Borrmann, S.: Design of a mobile aerosol research laboratory and data processing tools for effective stationary and mobile field measurements, Atmos. Meas. Tech., 5, 1443–1457, doi:10.5194/amt-5-1443-2012, 2012.

Dunlea, E. J., Herndon, S. C., Nelson, D. D., Volkamer, R. M., San Martini, F., Sheehy, P. M., Zahniser, M. S., Shorter, J. H., Wormhoudt, J. C., Lamb, B. K., Allwine, E. J., Gaffney, J. S., Marley, N. A., Grutter, M., Marquez, C., Blanco, S., Cardenas, B., Retama, A., Ramos Villegas, C. R., Kolb, C. E., Molina, L. T., and Molina, M. J.: Evaluation of nitrogen dioxide chemiluminescence monitors in a polluted urban environment, Atmos. Chem. Phys., 7, 2691–2704, doi:10.5194/acp-7-2691-2007, 2007.

Freney, E. J., Sellegri, K., Canonaco, F., Boulon, J., Hervo, M., Weigel, R., Pichon, J. M., Colomb, A., Prévôt, A. S. H., and Laj, P.: Seasonal variations in aerosol particle composition at the puy-de-Dôme research station in France, Atmos. Chem. Phys., 11, 13047–13059, doi:10.5194/acp-11-13047-2011, 2011.

Gros, V., Gaimoz, C., Herrmann, F., Custer, T., Williams, J., Bonsang, B., Sauvage, S., Locoge, N., d'Argouges, O., Sarda-Estève, R., and Sciare, J.: Volatile organic compounds sources in Paris in spring 2007. Part I: qualitative analysis, Environ. Chem., 8, 74–90, doi:10.1071/en10068, 2011.

Haeffelin, M., Barthès, L., Bock, O., Boitel, C., Bony, S., Bouniol, D., Chepfer, H., Chiriaco, M., Cuesta, J., Delanoë, J., Drobinski, P., Dufresne, J.-L., Flamant, C., Grall, M., Hodzic, A., Hourdin, F., Lapouge, F., Lemaître, Y., Mathieu, A., Morille, Y., Naud, C., Noël, V., O'Hirok, W., Pelon, J., Pietras, C., Protat, A., Romand, B., Scialom, G., and Vautard, R.: SIRTA, a ground-based atmospheric observatory for cloud and aerosol research, Ann. Geophys., 23, 253–275, doi:10.5194/angeo-23-253-2005, 2005.

Haeffelin, M., Angelini, F., Morille, Y., Martucci, G., Frey, S., Gobbi, G. P., Lolli, S., O'Dowd, C. D., Sauvage, L., Xueref-Rémy, I., Wastine, B., and Feist, D. G.: Evaluation of Mixing-Height Retrievals from Automatic Profiling Lidars and Ceilometers in View of Future Integrated Networks in Europe, Bound.-Lay. Meteorol., 143, 49–75, doi:10.1007/s10546-011-9643-z, 2012.

Harrison, R. M., Dall'Osto, M., Beddows, D. C. S., Thorpe, A. J., Bloss, W. J., Allan, J. D., Coe, H., Dorsey, J. R., Gallagher, M., Martin, C., Whitehead, J., Williams, P. I., Jones, R. L., Langridge, J. M., Benton, A. K., Ball, S. M., Langford, B., Hewitt, C. N., Davison, B., Martin, D., Petersson, K. F., Henshaw, S. J., White, I. R., Shallcross, D. E., Barlow, J. F., Dunbar, T., Davies, F., Nemitz, E., Phillips, G. J., Helfter, C., Di Marco, C. F., and Smith, S.: Atmospheric chemistry and physics in the atmosphere of a developed megacity (London): an overview of the REPARTEE experiment and its conclusions, Atmos. Chem. Phys., 12, 3065–3114, doi:10.5194/acp-12-3065-2012, 2012.

He, L.-Y., Lin, Y., Huang, X.-F., Guo, S., Xue, L., Su, Q., Hu, M., Luan, S.-J., and Zhang, Y.-H.: Characterization of high-resolution aerosol mass spectra of primary organic aerosol emissions from Chinese cooking and biomass burning, Atmos. Chem. Phys., 10, 11535–11543, doi:10.5194/acp-10-11535-2010, 2010.

Hersey, S. P., Craven, J. S., Schilling, K. A., Metcalf, A. R., Sorooshian, A., Chan, M. N., Flagan, R. C., and Seinfeld, J. H.: The Pasadena Aerosol Characterization Observatory (PACO): chemical and physical analysis of the Western Los Angeles basin aerosol, Atmos. Chem. Phys., 11, 7417–7443, doi:10.5194/acp-11-7417-2011, 2011.

Hill, M. K.: Understanding Environmental Pollution, 3rd ed., Cambridge University Press, Cambridge, 2010.

Hinds, W. C.: Aerosol technology: properties, behavior, and measurement of airborne particles, 2nd ed., John Wiley & Sons, Inc., New York, 1999.

Jimenez, J. L., Canagaratna, M. R., Donahue, N. M., Prevot, A. S. H., Zhang, Q., Kroll, J. H., DeCarlo, P. F., Allan, J. D., Coe, H., Ng, N. L., Aiken, A. C., Docherty, K. S., Ulbrich, I. M., Grieshop, A. P., Robinson, A. L., Duplissy, J., Smith, J. D., Wilson, K. R., Lanz, V. A., Hueglin, C., Sun, Y. L., Tian, J., Laaksonen, A., Raatikainen, T., Rautiainen, J., Vaattovaara, P., Ehn, M., Kulmala, M., Tomlinson, J. M., Collins, D. R., Cubison, M. J., Dunlea, E. J., Huffman, J. A., Onasch, T. B., Alfarra, M. R., Williams, P. I., Bower, K., Kondo, Y., Schneider, J., Drewnick, F., Borrmann, S., Weimer, S., Demerjian, K., Salcedo, D., Cottrell, L., Griffin, R., Takami, A., Miyoshi, T., Hatakeyama, S., Shimono, A., Sun, J. Y., Zhang, Y. M., Dzepina, K., Kimmel, J. R., Sueper, D., Jayne, J. T., Herndon, S. C., Trimborn, A. M., Williams, L. R., Wood, E. C., Middlebrook, A. M., Kolb, C. E., Baltensperger, U., and Worsnop, D. R.: Evolution of Organic Aerosols in the Atmosphere, Science, 326, 1525–1529, doi:10.1126/science.1180353, 2009.

Kunkel, D., Lawrence, M. G., Tost, H., Kerkweg, A., Jöckel, P., and Borrmann, S.: Urban emission hot spots as sources for remote aerosol deposition, Geophys. Res. Lett., 39, L01808, doi:10.1029/2011gl049634, 2012.

Lawrence, M. G., Butler, T. M., Steinkamp, J., Gurjar, B. R., and Lelieveld, J.: Regional pollution potentials of megacities and other major population centers, Atmos. Chem. Phys., 7, 3969–3987, doi:10.5194/acp-7-3969-2007, 2007.

Liu, P. S. K., Deng, R., Smith, K. A., Williams, L. R., Jayne, J. T., Canagaratna, M. R., Moore, K., Onasch, T. B., Worsnop, D. R., and Deshler, T.: Transmission Efficiency of an Aerodynamic Focusing Lens System: Comparison of Model Calculations and Laboratory Measurements for the Aerodyne Aerosol Mass Spectrometer, Aerosol Sci. Technol., 41, 721–733, doi:10.1080/02786820701422278, 2007.

Matthew, B. M., Middlebrook, A. M., and Onasch, T. B.: Collection Efficiencies in an Aerodyne Aerosol Mass Spectrometer as a Function of Particle Phase for Laboratory Generated Aerosols, Aerosol Sci. Technol., 42, 884–898, doi:10.1080/02786820802356797, 2008.

Menut, L., Vautard, R., Flamant, C., Abonnel, C., Beekmann, M., Chazette, P., Flamant, P. H., Gombert, D., Guédalia, D., Kley, D., Lefebvre, M. P., Lossec, B., Martin, D., Mégie, G., Perros, P., Sicard, M., and Toupance, G.: Measurements and modelling of atmospheric pollution over the Paris area: an overview of the ESQUIF Project, Ann. Geophys., 18, 1467–1481, doi:10.1007/s00585-000-1467-y, 2000.

Meteo France, http://worldweather.wmo.int/062/c00194.htm, last access: November 2011.

Molina, L. T., Madronich, S., Gaffney, J. S., Apel, E., de Foy, B., Fast, J., Ferrare, R., Herndon, S., Jimenez, J. L., Lamb, B., Osornio-Vargas, A. R., Russell, P., Schauer, J. J., Stevens, P. S., Volkamer, R., and Zavala, M.: An overview of the MILAGRO 2006 Campaign: Mexico City emissions and their transport and transformation, Atmos. Chem. Phys., 10, 8697–8760, doi:10.5194/acp-10-8697-2010, 2010.

Molina, M. J. and Molina, L. T.: Megacities and Atmospheric Pollution, J. Air Waste Manage. Assoc., 54, 644–680, 2004.

Orsini, D. A., Ma, Y., Sullivan, A., Sierau, B., Baumann, K., and Weber, R. J.: Refinements to the particle-into-liquid sampler (PILS) for ground and airborne measurements of water soluble

aerosol composition, Atmos. Environ., 37, 1243–1259, 2003.

Paatero, P.: Least squares formulation of robust non-negative factor analysis, Chemometrics and Intelligent Laboratory Systems, 37, 23–35, 1997.

Paatero, P. and Tapper, U.: Positive matrix factorization: A non-negative factor model with optimal utilization of error estimates of data values, Environmetrics, 5, 111–126, doi:10.1002/env.3170050203, 1994.

Salcedo, D., Onasch, T. B., Dzepina, K., Canagaratna, M. R., Zhang, Q., Huffman, J. A., DeCarlo, P. F., Jayne, J. T., Mortimer, P., Worsnop, D. R., Kolb, C. E., Johnson, K. S., Zuberi, B., Marr, L. C., Volkamer, R., Molina, L. T., Molina, M. J., Cardenas, B., Bernabé, R. M., Márquez, C., Gaffney, J. S., Marley, N. A., Laskin, A., Shutthanandan, V., Xie, Y., Brune, W., Lesher, R., Shirley, T., and Jimenez, J. L.: Characterization of ambient aerosols in Mexico City during the MCMA-2003 campaign with Aerosol Mass Spectrometry: results from the CENICA Supersite, Atmos. Chem. Phys., 6, 925–946, doi:10.5194/acp-6-925-2006, 2006.

Sciare, J., d'Argouges, O., Zhang, Q. J., Sarda-Estève, R., Gaimoz, C., Gros, V., Beekmann, M., and Sanchez, O.: Comparison between simulated and observed chemical composition of fine aerosols in Paris (France) during springtime: contribution of regional versus continental emissions, Atmos. Chem. Phys., 10, 11987–12004, doi:10.5194/acp-10-11987-2010, 2010.

Seinfeld, J. H. and Pandis, S. N.: Atmospheric Chemistry and Physics: From Air Pollution to Climate Change, 2nd ed., John Wiley & Sons, Inc., New York, 2006.

Stohl, A., Forster, C., Frank, A., Seibert, P., and Wotawa, G.: Technical note: The Lagrangian particle dispersion model FLEXPART version 6.2, Atmos. Chem. Phys., 5, 2461–2474, doi:10.5194/acp-5-2461-2005, 2005.

Sun, J., Zhang, Q., Canagaratna, M. R., Zhang, Y., Ng, N. L., Sun, Y., Jayne, J. T., Zhang, X., Zhang, X., and Worsnop, D. R.: Highly time- and size-resolved characterization of submicron aerosol particles in Beijing using an Aerodyne Aerosol Mass Spectrometer, Atmos. Environ., 44, 131–140, doi:10.1016/j.atmosenv.2009.03.020, 2010.

Sun, Y.-L., Zhang, Q., Schwab, J. J., Demerjian, K. L., Chen, W.-N., Bae, M.-S., Hung, H.-M., Hogrefe, O., Frank, B., Rattigan, O. V., and Lin, Y.-C.: Characterization of the sources and processes of organic and inorganic aerosols in New York city with a high-resolution time-of-flight aerosol mass apectrometer, Atmos. Chem. Phys., 11, 1581–1602, doi:10.5194/acp-11-1581-2011, 2011.

Takegawa, N., Miyakawa, T., Kondo, Y., Blake, D. R., Kanaya, Y., Koike, M., Fukuda, M., Komazaki, Y., Miyazaki, Y., Shimono, A., and Takeuchi, T.: Evolution of submicron organic aerosol in polluted air exported from Tokyo, Geophys. Res. Lett., 33, L15814, doi:10.1029/2006gl025815, 2006a.

Takegawa, N., Miyakawa, T., Kondo, Y., Jimenez, J. L., Zhang, Q., Worsnop, D. R., and Fukuda, M.: Seasonal and diurnal variations of submicron organic aerosol in Tokyo observed using the Aerodyne aerosol mass spectrometer, J. Geophys. Res., 111, D11206, doi:10.1029/2005jd006515, 2006b.

Tuch, T. M., Haudek, A., Müller, T., Nowak, A., Wex, H., and Wiedensohler, A.: Design and performance of an automatic regenerating adsorption aerosol dryer for continuous operation at monitoring sites, Atmos. Meas. Tech., 2, 417–422, doi:10.5194/amt-2-417-2009, 2009.

Ulbrich, I. M., Canagaratna, M. R., Zhang, Q., Worsnop, D. R., and Jimenez, J. L.: Interpretation of organic components from Positive Matrix Factorization of aerosol mass spectrometric data, Atmos. Chem. Phys., 9, 2891–2918, doi:10.5194/acp-9-2891-2009, 2009.

Ulbrich, I. M., Canagaratna, M. R., Cubison, M. J., Zhang, Q., Ng, N. L., Aiken, A. C., and Jimenez, J. L.: Three-dimensional factorization of size-resolved organic aerosol mass spectra from Mexico City, Atmos. Meas. Tech., 5, 195–224, doi:10.5194/amt-5-195-2012, 2012.

UN DESA, United Nations Department of Economic and Social Affairs, Population Division: World Population Prospects: The 2008 Revision: http://esa.un.org/wup2009/unup/index.asp (last access: November 2011), 2008.

UN DESA, United Nations Department of Economic and Social Affairs, Population Division: World Urbanization Prospects: The 2009 Revision: http://esa.un.org/wup2009/unup/index.asp (last access: November 2011), 2009.

van Pinxteren, D., Brüggemann, E., Gnauk, T., Iinuma, Y., Müller, K., Nowak, A., Achtert, P., Wiedensohler, A., and Herrmann, H.: Size- and time-resolved chemical particle characterization during CAREBeijing-2006: Different pollution regimes and diurnal profiles, J. Geophys. Res., 114, D00G09, doi:10.1029/2008jd010890, 2009.

Vautard, R., Menut, L., Beekmann, M., Chazette, P., Flamant, P. H., Gombert, D., Guédalia, D., Kley, D., Lefebvre, M.-P., Martin, D., Mégie, G., Perros, P., and Toupance, G.: A synthesis of the Air Pollution Over the Paris Region (ESQUIF) field campaign, J. Geophys. Res., 108, 8558, doi:10.1029/2003jd003380, 2003.

von der Weiden, S.-L., Drewnick, F., and Borrmann, S.: Particle Loss Calculator – a new software tool for the assessment of the performance of aerosol inlet systems, Atmos. Meas. Tech., 2, 479–494, doi:10.5194/amt-2-479-2009, 2009.

von der Weiden-Reinmüller, S.-L., Drewnick, F., Zhang, Q. J., Freutel, F., Beekmann, M., and Borrmann, S.: Megacity emission plume characteristics in summer and winter investigated by mobile aerosol and trace gas measurements: The Paris metropolitan area, to be submitted to Atmos. Chem. Phys. Discuss., 2013.

Wang, T., Nie, W., Gao, J., Xue, L. K., Gao, X. M., Wang, X. F., Qiu, J., Poon, C. N., Meinardi, S., Blake, D., Wang, S. L., Ding, A. J., Chai, F. H., Zhang, Q. Z., and Wang, W. X.: Air quality during the 2008 Beijing Olympics: secondary pollutants and regional impact, Atmos. Chem. Phys., 10, 7603–7615, doi:10.5194/acp-10-7603-2010, 2010.

Weimer, S., Drewnick, F., Hogrefe, O., Schwab, J. J., Rhoads, K., Orsini, D., Canagaratna, M., Worsnop, D. R., and Demerjian, K. L.: Size-selective nonrefractory ambient aerosol measurements during the Particulate Matter Technology Assessment and Characterization Study - New York 2004 Winter Intensive in New York City, J. Geophys. Res., 111, D18305, doi:10.1029/2006jd007215, 2006.

Widory, D., Roy, S., Le Moullec, Y., Goupil, G., Cocherie, A., and Guerrot, C.: The origin of atmospheric particles in Paris: a view through carbon and lead isotopes, Atmos. Environ., 38, 953–961, 2004.

Xing, J.-H., Takahashi, K., Yabushita, A., Kinugawa, T., Nakayama, T., Matsumi, Y., Tonokura, K., Takami, A., Imamura, T., Sato, K., Kawasaki, M., Hikida, T., and Shimono, A.: Characterization

of Aerosol Particles in the Tokyo Metropolitan Area using Two Different Particle Mass Spectrometers, Aerosol Sci. Technol., 45, 315–326, 2011.

Zhang, Q., Worsnop, D. R., Canagaratna, M. R., and Jimenez, J. L.: Hydrocarbon-like and oxygenated organic aerosols in Pittsburgh: insights into sources and processes of organic aerosols, Atmos. Chem. Phys., 5, 3289–3311, doi:10.5194/acp-5-3289-2005, 2005.

Zhang, Q., Jimenez, J. L., Canagaratna, M. R., Ulbrich, I. M., Ng, N. L., Worsnop, D. R., and Sun, Y.: Understanding atmospheric organic aerosols via factor analysis of aerosol mass spectrometry: a review, Analytical and Bioanalytical Chemistry, 401, 3045–3067, doi:10.1007/s00216-011-5355-y, 2011.

Zorn, S. R., Drewnick, F., Schott, M., Hoffmann, T., and Borrmann, S.: Characterization of the South Atlantic marine boundary layer aerosol using an aerodyne aerosol mass spectrometer, Atmos. Chem. Phys., 8, 4711–4728, doi:10.5194/acp-8-4711-2008, 2008.